



## GEOSCIENCES

# Water stable isotopes in snow along a traverse of the West Antarctic Ice Sheet: insights into moisture origins, air-masses distillation history, and climatic value

ANDRESSA MARCHER, RONALDO T. BERNARDO, JEFFERSON C. SIMÕES & JEFFREY AUGER

**Abstract:** This study investigated the water isotopic content ( $\delta^{18}\text{O}$ ,  $\delta\text{D}$ , d-excess) of the surface snow along a 995 km traverse over the West Antarctic Ice Sheet from the Möller Ice Stream – Institute Ice Stream to the upper reaches of the Pine Island Glacier drainage basin. The purpose of this study was to evaluate the climatic record preserved in the snow. We analyzed 92 surface samples (~0.15–0.20 m deep), retrieved during 2014/2015 austral summer from every ~10 km along the traverse route, using the laser spectroscopy technique. We computed the isotopic-geographical characteristics and spatial co-isotopic empirical relationships and compared the isotopic results with the tropospheric mean annual temperature and air mass trajectories. Our isotopic results were sensitive to capturing the well-known climatic asymmetry between the Amundsen-Bellinghousen Sea (ABS; which receives more influence from warmer (oceanic) air masses) and Weddell Sea (WS; more influenced by colder (continental) air masses) sectors. Further, the spatial distribution of  $\delta\text{s}$  and d-excess and the co-isotopic relationships reflect two preferential fractionation paths: one from the coast of the ABS sector to the WS sector, and another from the coast of the WS sector to the inland. The Pacific Ocean is confirmed as the primary source of moisture.

**Key words:** water stable isotopes, surface snow, isotopic fractionation, air masses, moisture origin, WAIS.

## INTRODUCTION

Understanding and monitoring the West Antarctic Ice Sheet (WAIS) climate is relevant owing to its sensitivity to ocean and atmospheric circulation changes. This sensitivity is primarily related to its morphology, as the WAIS is a maritime ice sheet; that is, the ice-bedrock interface is below sea level. Furthermore, it is topographically lower (mean altitude 1,100 m above sea level (a.s.l.); maximum around 2,200 m a.s.l.) than the East Antarctic Ice Sheet (EAIS; mean altitude of 2,835 m a.s.l.; maximum around 4,000 m a.s.l.) (Turner 2009, Bell & Seroussi 2020), which favors

the strong influence of oceanic air masses on its central region (Nicolas & Bromwich 2011). Over the last decade, it has become clear that such influence has a significant role in modulating the surface air temperature, precipitation, and cloud fractions on the WAIS (Nicolas & Bromwich 2009, 2011). Some studies (Nicolas & Bromwich 2011, Hosking et al. 2013, Raphael et al. 2016) have shown that the frequency and intensity of these maritime air incursions are tied to variations in the longitudinal position and deepening of the Amundsen Sea Low (ASL) (at monthly, seasonal, and annual scales). However, the variations

in the contribution of heat and moisture throughout the WAIS are not well understood (i.e., the climate history from various regions of WAIS is poorly known).

In recent decades, the WAIS glacial drainage basins in the Amundsen- Bellingshausen Sea Sector (ABS sector) have been retreating at high rates (Rignot et al. 2008, Pritchard et al. 2012, Shepherd et al. 2018). Superficial melting has been observed in these basins even in some winter months, although it is less expressive than the melting observed in the Antarctic Peninsula (Wille et al. 2019). It has been pointed out that such rare melting events are largely explained by the slight intensification of atmospheric river incursions in this region (Wille et al. 2019). Furthermore, radiosonde studies have identified significant warming of the Antarctic troposphere in winter since the late 1970s (Turner et al. 2006, Ding et al. 2011), and meteorological station data from the Amundsen-Ross Sea Sector and Peninsula have shown a significant surface warming trend in West Antarctica from the 20<sup>th</sup> century onwards (Steig et al. 2009, Bromwich et al. 2013). In comparison, the Weddell Sea Sector (WS sector) drainage basins (Institute Ice Stream (IIS), Möller Ice Stream (MIS), and others) are currently stable (Siegert et al. 2019), and there is still no evidence of surface melting events in winter months. Moreover, no mean annual temperature trends in the 21<sup>st</sup>-century have been observed in the Antarctic Peninsula (Turner et al. 2016) or WS sector (Pinto 2017, Hoffmann et al. 2020). However, there is some evidence of warm and wet air incursions in winters at the automatic scientific module Criosfera 1 (84° S, 79.5° W) in the WS sector (Pinto 2017).

These recent temporal and spatial contrasts between different sectors accentuate the importance of a deeper understanding of climate variability in each WAIS sector and subsector (at the glacial drainage basin scale). However,

such knowledge is hampered by the scarce, long-spaced, and incomplete instrumental records from automatic weather stations and the limited temporal cover of satellite data. To overcome these limitations, the use of proxy data (precipitation, snow, and ice chemistry) has proved to be an essential tool for obtaining climatic information, with the water isotopic content being the most frequently used proxy.

The stable isotope composition of water is one of the most important and frequently used proxies of condensation temperature (information extracted from  $\delta^{18}\text{O}$  and  $\delta\text{D}$  series) and moisture source conditions (information extracted from  $d$ -excess, which is a second-order parameter obtained from the relation between  $\delta s$  given by  $d = \delta\text{D} - 8 \times \delta^{18}\text{O}$ ) (Masson-Delmotte et al. 2008, Hou et al. 2013, Jouzel 2013). The  $\delta^{18}\text{O}$  and  $\delta\text{D}$  ratios are a consequence from the  $\delta$ -depletion as the air masses cool and advance toward Antarctica's interior. The  $d$ -excess results from non-equilibrium processes that occur in the moisture source region.

Since the pioneering studies in the 1950–70s (Epstein & Mayeda 1953, Epstein et al. 1963, Dansgaard 1954, 1964, Dansgaard et al. 1973), the water isotope potential for paleoclimatic studies has been extensively explored by deep ice core research communities to reconstruct the Quaternary climate history in East Antarctica (Petit et al. 1999, Vimeux et al. 1999, EPICA community members 2004, Jouzel et al. 2007) and West Antarctica (Johnsen et al. 1972, WAIS Divide Project Members 2013) regions. In West Antarctica, a record of approximately 68–80,000 years BP (before 1950) of climatic history was recovered from the Byrd region (Johnsen et al. 1972, WAIS Divide Project Members 2013). Over the past two decades, many other water isotope time series have been recovered, including shallow firn and ice cores along transects (Schneider & Steig 2008, Küttell et al. 2012, Lindau et al.

2016) and at some specific sites (Schwanck et al. 2017, Hoffmann et al. 2020) across the WAIS. Most of these drillings have been encouraged by the International Trans-Antarctic Scientific Expeditions (ITASE; Mayewski & Goodwin 1997, Mayewski 2006), which aims to understand climate variability in recent centuries (over the past 200 years) at a regional scale.

Despite all these efforts, there is still a shortage of stable isotopic data from the WAIS, making it difficult to interpret the stable isotope record in ice cores. It is well known that the interpretation of stable isotope records in water environments is not straightforward, as many factors exert considerable influence on the isotopic content of precipitation, such as precipitation intermittency (Masson-Delmotte et al. 2008, Touzeau et al. 2016), transport path (Noone & Simmonds 2002, Noone 2008, Masson-Delmotte et al. 2008), sea ice, and moisture origin variations (Noone & Simmonds 2004, Sodemann & Stohl 2009). In addition, some post-depositional processes could also affect the original precipitation isotopic ratios, such as sublimation, wind-driven erosion, glaze ice, deep hoar formation, and the vapor-snow isotopic exchange between two precipitation events (Masson-Delmotte et al. 2008, Neumann et al. 2008, Marquetto et al. 2015, Ritter et al. 2016, Bréant et al. 2019). The scarcity of documentation and challenges highlight the importance of evaluating how climatic signals are preserved on surface snow in recent times and in different regions of Antarctica to identify the quality of the climatic signal and possible post-depositional processes that operate in a particular ice core area.

In this context, we studied the isotopic data of the surface snow collected along a 2014 traverse in the upstream areas of three WAIS glacial drainage basins (PIG, IIS, and MIS). This study aimed to (1) identify the

preferential fractionation paths (i.e., improve our understanding of the trajectory effect on the isotopic composition in the studied area), (2) infer the moisture sources that most influenced the stable isotopic composition of surface snow, and (3) determine the climatic and non-climatic factors that may affect snow isotopic signals in these areas. Accordingly, the approach to achieving these three objectives is outlined. First, we determined the empirical relationships between stable isotope composition and geographical parameters and the co-isotopic relationships. Second, we compared the isotopic trends with the 2014 tropospheric mean temperature and snow precipitation data obtained from ERA5 solutions (CDS (C3S) 2017), and also with the air mass trajectories, which were simulated for ten sites using the Hybrid Single-Particle Lagrangian Integrated Trajectory (HYSPLIT) model (Draxler & Hess 1998, Stein et al. 2015).

## MATERIALS AND METHODS

### Study area and the 2015 Brazilian traverse of the West Antarctic Ice Sheet

A Brazilian traverse of the WAIS (hereafter, BR-WAIS traverse) was carried out in the 2014–2015 austral summer (January 4–21) by a research group from the Centro Polar e Climático (Polar and Climatic Center) of the Federal University of Rio Grande do Sul (CPC/UFRGS). Our team covered a 1,700 km route traversing over the upper reaches of three glacial drainage basins: the PIG basin (ABS sector), IIS, and MIS basins (WS sector) (Fig. 1).

The BR-WAIS traverse started at the base camp on the Union Glacier (Ellsworth Mountains; 79°46'00" S, 82°50'00" W) and sampling began at (1) the Brazilian automatic scientific module Criosfera 1 (S01 sample, position 84°00'00" S, 79°29'39" W), where the first sampling of

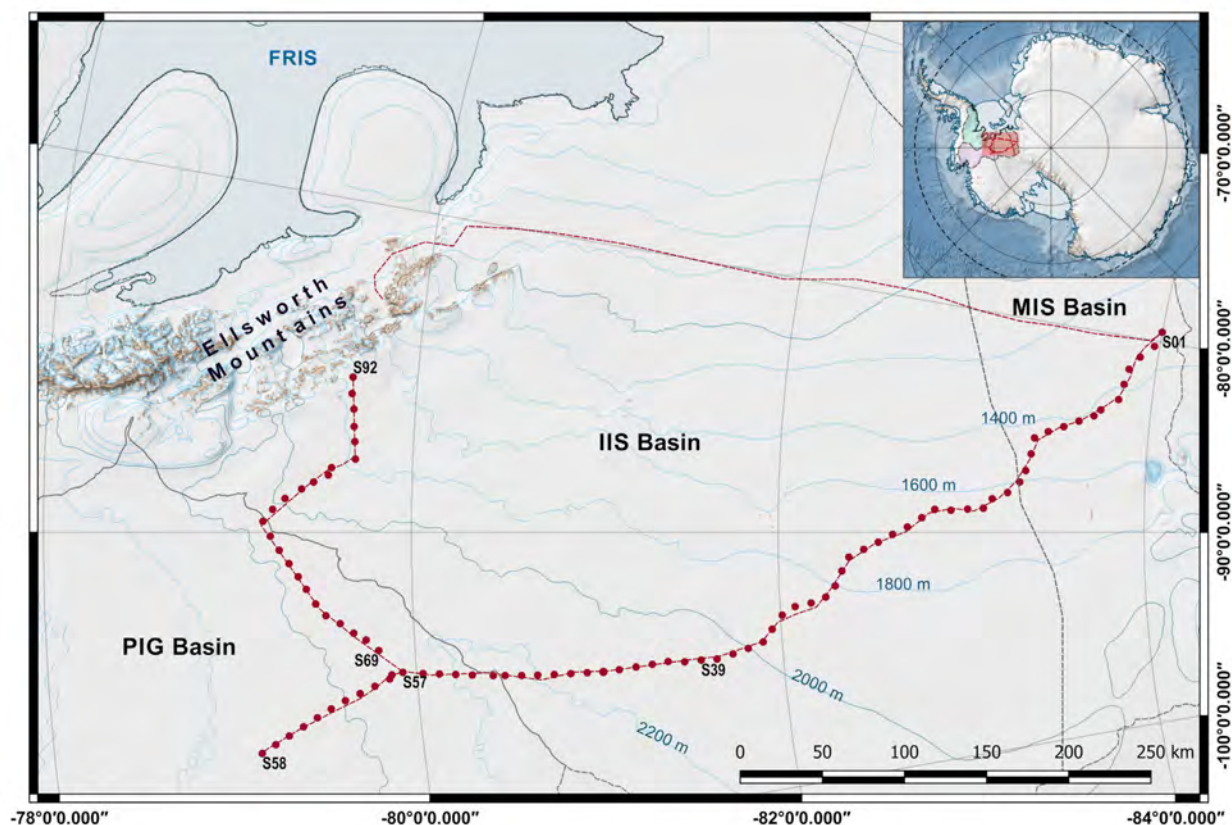


**Figure 1.** Map showing the route (thin red line) of the 2015 Brazilian traverse on the West Antarctic Ice Sheet (WAIS). Red dots are the surface snow samples sites. The red dashed line is the non-sampled route from Ellsworth Mountains to the Criosfera 1 scientific module site. Gray contours represent the basin boundaries. Blue lines represent terrain contours at every 200 m height. This map is made in QGIS using the Quantarctica 3 Project datasets (Matsuoka et al. 2018).

superficial snow and a shallow ice core (at the same position) were retrieved; from there to (2) the site where a Mount Johns ice core was recovered (S57 sample position; 79°55'00\" S, 94°23'00\" W) in the 2008–09 austral summer; and to (3) Ellsworth Mountains region, where the last sample was collected (S92; 79°38'58.0\" S, 85°18'09.0\" W). In addition, an exploratory route (of approximately 110 km) was carried out from the Mount Johns site downstream of the PIG basin, reaching the coordinates 79°07'23.3\" S, 96°22'30.06\" W (S58 sample position).

During all traverse days, the meteorological conditions were clear skies, mild wind, and temperatures between -10 °C and -22 °C, favoring the sampling process. In the MIS basin [from

sampling site S01 (84°00'00\" S, 79°29'39\" W) to ~ S15 (83°18'56.5\" S, 87°38'17.8\" W)], we crossed sastrugi fields of 20–40 cm amplitude. In the other basins, we observed only soft snow with few wind features.

### Surface snow sample collection

Along the BR-WAIS traverse route, 92 surface snow samples were collected, approximately every 10 km, with eight shallow ice cores, ranging from 5 to 21 m deep. This study only discusses the surface sample results. Figure 1 shows the surface snow sampling sites (site data for each sample are shown in the Supplementary Material - Table SI). Gloves, a plastic head shovel, and polyethylene bottles previously washed with

ultrapure water (produced by a MilliQ system) were used to collect surface snow samples. The sampling procedure consisted of a small pit (approximately 30 cm deep), wide enough for a bottle to be placed and pressed against the bottom and then pulled up (sampling ~15–20 cm of the surface snow). All samples were stored in high-density Styrofoam boxes and kept frozen until melted for the isotope analysis to ensure original isotopic content conservation.

### Water stable isotope analysis

The samples were analyzed at the CPC/UFRGS Stable Isotope Lab using a wavelength-scanned cavity ring-down spectroscopy (WS-CRDS) analyzer (model L2130-i, PICARRO® Inc., USA; www.picarro.com). The 92 samples were distributed in four rounds of analysis. Before each round, a batch of approximately 23 samples were thawed on the lab bench. After thawing, 2 ml sample aliquots were transferred to top screw cleanglass vials (2 ml). Subsequently, these were sealed with screw caps containing PTFE/silicone septa (9 mm) to prevent isotopic fractionation by evaporation. Four water laboratory secondary standards, previously calibrated against the international scale [Vienna Standard Mean Ocean Water (VSMOW2), Greenland Ice Sheet Precipitation (GISP), and Standard Light Antarctic Precipitation (SLAP2)], were analyzed with each batch of samples to correct the analyzer drift. Eight injections were administered to each vial during the analysis. After the analysis, we discarded the first five results and calculated the average of the other three to eliminate the memory effect. We calibrated all raw isotope data using linear regression analysis using the laboratory standards values. Finally, we computed deuterium excess (d-excess) values by the standard definition:

$$d = \delta D - 8 \times \delta^{18}O \text{ (Dansgaard 1964).}$$

The results are in the  $\delta$ -notation ( $\delta D$  and  $\delta^{18}O$ ) – deviation per mille (‰) of the sample isotopic ratios ( $R = D/H$  and  $^{18}O/^{16}O$ ) in relation to the isotopic ratios ( $R$ ) from the reference standard VSMOW (Vienna Standard Mean Ocean Water), according to the equation:

$$\delta_{(sample)} = \left( \frac{R_{(sample)}}{R_{(VSMOW)}} - 1 \right) \times 1000 (\text{‰})$$

The accuracy of the measurements is 0.8 ‰ for  $\delta D$  and 0.2 ‰ for  $\delta^{18}O$ .

### Determination of empirical relationships

After the isotopic analysis and correction procedures, we used a linear regression model to verify the empirical relationships of the water stable isotope ratios with geographical parameters (latitude, longitude, altitude, and distance to coast (from the PIG coastline)) and the co-isotopic relationships ( $\delta D$ - $\delta^{18}O$  and d-excess- $\delta s$ ). Generally, Antarctic surface snow studies describe the isotopic composition variability using geographical parameters that indirectly represent changes in the condensation temperature (the fundamental factor that determines isotopic compositions in polar regions) and that affect air mass distillation (Dahe et al. 1994, Masson-Delmotte et al. 2008, Kang et al. 2009, Wang et al. 2010, Xiao et al. 2013, Hou et al. 2013, Marquette et al. 2015). Usually, the following parameters are used: latitude, altitude, and distance from the coast. However, in our investigation, we also considered longitude to be a significant geographical parameter because the air masses that penetrate over the WAIS rotate cyclonically (Nicolas & Bromwich 2009) and, therefore, west-east isotopic depletion may occur (Masson-Delmotte et al. 2008). Co-isotopic relations are essential for checking the quality of the samples and evaluating the isotopic fractionation.

## Meteorological data

The temperatures at 14 pressure levels (ranging from 1000 to 600 hPa) along the traverse route and monthly snow precipitation data for 11 sites (S01, S10, S20, S30, S40, S50, S57, S58, S70, S80, and S92) were taken from the European Center for Medium-Ranged Weather Forecasts (ECMWF) Reanalysis 5 datasets. We constructed two tropospheric temperature vertical cross-sections with ERA5 model solutions to examine the 2014 mean annual tropospheric temperature throughout the sampled transects (N-S and E-W). For this purpose, the mean temperature for the lower troposphere was calculated by averaging the monthly mean of 2014.

We used the 2014 monthly total precipitation data to identify the wet months and monthly snow precipitation distribution variability along the route. Such identification is important for two reasons: (1) it allows the identification of the seasons that weigh most in the isotopic composition of snow, and (2) it allows the definition of zones with the same precipitation pattern, which in turn allows a better understanding of the paths of air masses and moisture sources.

The ERA5 temperatures at different pressure levels were obtained from the Climate Data Store hosted by Copernicus (CDS (C3S) 2017; available at <https://cds.climate.copernicus.eu/cdsapp#!/home>; last access: October 2019), while the precipitation data were obtained from the Climate Reanalyzer.org (CCI/UMaine; available at: [https://climatereanalyzer.org/reanalysis/monthly\\_tseries/](https://climatereanalyzer.org/reanalysis/monthly_tseries/); last accessed: January 2021; the data are listed in the Table SII). We chose to use the reanalysis data because there were few automatic weather stations (AWSs) along this route. ERA5 is the latest release of all reanalysis models. It has been improved substantially since the ECMWF last release (ERA-Interim, Dee et al. 2011), including higher spatial (with a lat-long

grid of 0.25° and 37 pressure levels) and temporal (from 1950 to present) resolutions and better global precipitation and evaporation balances (Hersbach & Dee 2016, Hersbach et al. 2019). Based on Tetzer et al. (2019), ERA5 data perform well in areas above 1000 m of altitude and effectively represent the meteorological variability in the ABS sector. This good representation is also confirmed in the WS sector by comparing the ERA5 results with meteorological data from the Criosfera 1 automatic module (unpublished data from the CPC/UFRGS). As the ERA5 data showed considerable warm biases, we interpreted temperature variations in comparative terms only.

## Air mass backward trajectories calculation

We used the Hybrid Single-Particle Lagrangian Integrated Trajectory (HYSPPLIT) v4 model, developed by the NOAA Air Resources Laboratory (Draxler & Hess 1998, Stein et al. 2015; available at: <https://www.ready.noaa.gov/HYSPLIT.php>) to evaluate the variation in air mass transport and principal moisture origin along the BR-WAIS route. For this purpose, we ran the model for ten sites (S01, S10, S20, S30, S40, S50, S58, S70, S80, and S92) approximately equally spaced (~100 km). This model has been used in previous studies of the WAIS to understand the synoptic controls on precipitation and transport of aerosols to the Mount Johns area (Schwanck et al. 2016, 2017, Marquette et al. 2020), to develop a proxy for synoptic variability using chemical records of the ice cores from the Ross Sea sector (hereafter RS sector) (Dixon et al. 2012, Markle et al. 2012), to confirm the origin of air masses arriving at the Criosfera 1 module (Pinto 2017), and to identify the source of moisture in the precipitation in the WS sector (Marquette et al. 2015, Hoffmann et al. 2020).

The model was run with a 10-day (240 h) backward calculation every 6 h to create

three-dimensional back-trajectories arriving at the BR-WAIS traverse region throughout 2014. The trajectories were simulated for 1000 m above the ground level. We used global meteorological data from the National Center for Environmental Prediction and the National Center for Atmospheric Research reanalysis (NCEP/NCAR reanalysis; Kalnay et al. 1996). These reanalysis data are available on the Ready NOAA website (<https://www.ready.noaa.gov/archives.php>, last access: January 2021).

For each site, 1460 trajectories were produced and then stored in distinct directories for cluster analysis according to the season (wet and dry). In this work, we considered the autumn and winter months (i.e., March–August 2014) as the wet season and the summer and spring months (i.e., January–February and September–December 2014) as the dry season. After the HYSPLIT cluster analysis was applied to the database of the individual trajectories, we recognized six clusters as an appropriate number to capture the seasonal variability of the airflow pattern for the 10-day back-trajectory simulations at all sites. This choice was based on (1) the analysis of the total spatial variance (TSV (%)) change as clusters were combined; (2) the evaluation of the 30% change criterion (Table SIII); and (3) the test with three different cluster numbers (7, 6, and 5) before the detachable TSV increased. We used 724 trajectories in the clustering procedure for the dry season and 736 trajectories for the wet season. The model results were saved in Shapefile format and subsequently plotted using QGIS software.

Because moisture sources for the Antarctic Ice Sheet are mainly located at mid- latitudes and near the sea ice boundary (Petit et al. 1991, Delaygue et al. 2000, Noone & Simmonds 2002, Masson-Delmotte 2008, Sodemann & Stohl 2009), we distinguished clusters originating from the open ocean from those from sea ice-covered

areas and the continent. To perform this classification, we consulted the sea ice extension (SIE) and sea ice concentration (SIC) 2014 data from the US National Snow and Ice Data Center ([www.nsidc.org](http://www.nsidc.org), last access: January 2021). Then, we refined our classification for oceanic or continental influence by evaluating the pattern, velocity (proportional to cluster length), height, pathway, and comparing the clusters obtained at each point (i.e., we analyzed the spatial relationship of clusters). After this classification, we computed the total contribution of the oceanic and continental air masses for both the wet and dry seasons for each site. The origin of the air masses was determined by evaluating which sector lies in the termination of the clusters. For this approach, a modified version of the Antarctic sector map of Goursaud et al. (2019) (Supplementary Material - Fig. S1) was used. Although this classification seems simplified because it ignored some trajectories, it was acceptable in our study scale because we worked with an annual isotopic average.

## RESULTS

### Surface snow results

Table SI lists the surface snow samples isotopic results. The S51 sample was the only outlier discarded because its  $\delta$  values were more enriched than its neighbors. As mentioned, we applied a linear regression model to define the empirical relationships between isotopic compositions and between them and geographic parameters. We opted to evaluate these relationships by transects and to present them according to the trend signal. Hence, we defined three transects: N-S transect (1) from the MIS basin to the southernmost part of the IIS basin, N-S transect (2) from the northernmost part of the IIS basin to the PIG basin, and E-W transect (3) from PIG basin to IIS basin (Ellsworth

Mountains). All coefficients obtained by Pearson correlation analysis (for each transect previously defined) are given in Table I, along with the extreme values of each isotopic parameter. Table SIV presents the slopes, intercepts, and determination coefficients of a linear model concerning geographic relationships.

The N-S transect (2) showed a statistically significant negative linear correlation of  $\delta s$  with the latitude [Lat, expressed in °S; -0.86 for  $\delta^{18}O$  ( $p < 0.001$ ) and -0.85 for  $\delta D$  ( $p < 0.001$ )] and the distance from the coast [Dist, expressed in km; -0.85 for  $\delta^{18}O$  ( $p < 0.001$ ) and -0.84 for  $\delta D$  ( $p < 0.001$ )] (Table I; Fig. 2a). The  $\delta$  values decreased with increasing latitude and continentality toward the PIG basin ice divide (ABS sector) to approximately 150 km within the IIS basin (WS Sector). From this distance to the Criosfera 1 automatic module site (N-S Transect (1); MIS basin), there was no  $\delta s$  isotopic trend ( $\delta^{18}O$ mean:  $-40.67 \pm 1.73 \text{ ‰}$ ;  $\delta D$ mean:  $-319.80 \pm 13.98 \text{ ‰}$ ),

although a difference of 800 m in altitude and 2.5° in latitude (Fig. 1, Fig. 2a).

The E-W transect (3) showed a moderate positive correlation of  $\delta s$  with the longitude [expressed in °W; 0.53 for  $\delta^{18}O$  ( $p = 0.001-0.01$ ) and 0.46 for  $\delta D$  ( $p = 0.01- 0.05$ )] and the altitude [expressed in m; 0.55 for  $\delta^{18}O$  ( $p = 0.001-0.01$ ) and 0.49 for  $\delta D$  ( $p = 0.01- 0.05$ )] (Table I; Fig. 2b). Moreover, the relationship between  $\delta s$  and the distance to coast had an inverse behavior [negative correlation; -0.58 for  $\delta^{18}O$  ( $p = 0.001-0.01$ ), and -0.53 for  $\delta D$  ( $p = 0.001-0.01$ )]. In other words,  $\delta s$  increased from the Ellsworth Mountains to the WAIS divide (ABS sector).

The d-excess, in both N-S (2) and E-W (3) transects, increased toward the WS sector, as shown by its correlation with the distance to the coast, statistically significant and positive in both transects [0.71 ( $p < 0.001$ ) in the N-S transect (2) and 0.76 ( $p < 0.001$ ) in the E-W transect (3)], along with the latitude ( $r = 0.72$ ,  $p < 0.001$ ) in the

**Table I. Top of the table: Linear correlation coefficients between isotopic content ( $\delta^{18}O$ ,  $\delta D$  and d-excess) and geographical parameters for each transect (a: N-S Transect (1) (south part); b: N-S Transect (2) (north part); c: E-W Transect (3)). Significant values (with a confidence level of 95.0%) are in bold. Bottom of the table: Maximum, minimum, mean (and standard deviation) values of the isotopic content for each transect.**

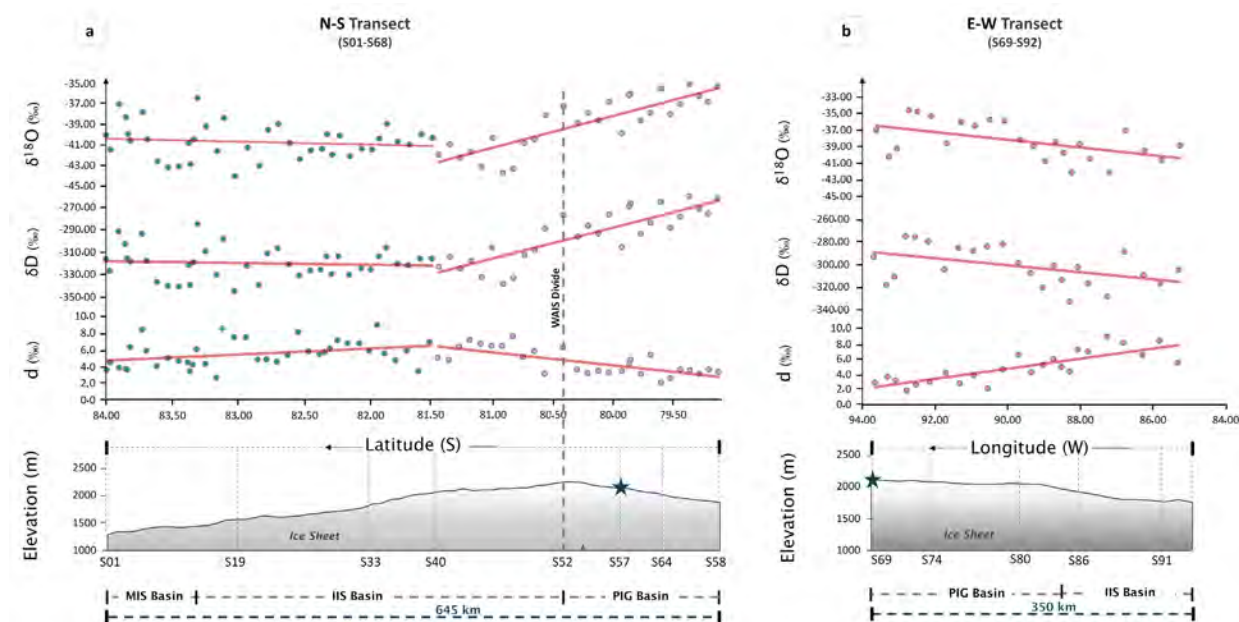
	N-S Transect						E-W Transect		
	(a) N-S transect (1): S01-S39			(b) N-S transect (2): S40-S68			(c) E-W transect (3): S69-S92		
	$\delta^{18}O$ (‰)	$\delta D$ (‰)	d (‰)	$\delta^{18}O$ (‰)	$\delta D$ (‰)	d (‰)	$\delta^{18}O$ (‰)	$\delta D$ (‰)	d (‰)
Lat (°S)	0.13	0.08	<b>-0.35*</b>	<b>-0.86**</b>	<b>-0.85**</b>	<b>0.72**</b>	-0.29	-0.29	0.21
Lon (°W)	-0.14	-0.09	<b>0.39*</b>	0.40	0.41	-0.27	<b>0.53*</b>	<b>0.46*</b>	<b>-0.82**</b>
Alt (m)	-0.06	-0.02	<b>0.36*</b>	-0.47	-0.47	0.39	<b>0.55*</b>	<b>0.49*</b>	<b>-0.82**</b>
Dist. (km)	0.13	-0.09	<b>-0.35*</b>	<b>-0.85**</b>	<b>-0.84**</b>	<b>0.71**</b>	<b>-0.58*</b>	<b>-0.53*</b>	<b>0.76**</b>
$\delta^{18}O$	1	<b>0.99**</b>	0.01	1	<b>1.00**</b>	<b>-0.73**</b>	1	<b>1.00**</b>	<b>-0.61*</b>
$\delta D$		1	0.13		1	<b>-0.70**</b>		1	<b>-0.52*</b>
Max	-36.42	-285.26	9.0	-35.19	-278.03	7.5	-34.60	-274.98	8.9
Mean	-40.67	-319.80	5.5	-38.78	-305.81	4.5	-38.30	-301.45	4.9
Min	-44.03	-344.78	2.7	-43.39	-340.81	2.0	-42.19	-332.64	1.8
SD	1.72	13.84	1.6	2.47	8.58	1.6	2.23	16.65	2.1

\* p: 0.01-0,05; \* p: 0.001-0.01; \*\* p: <0.001.

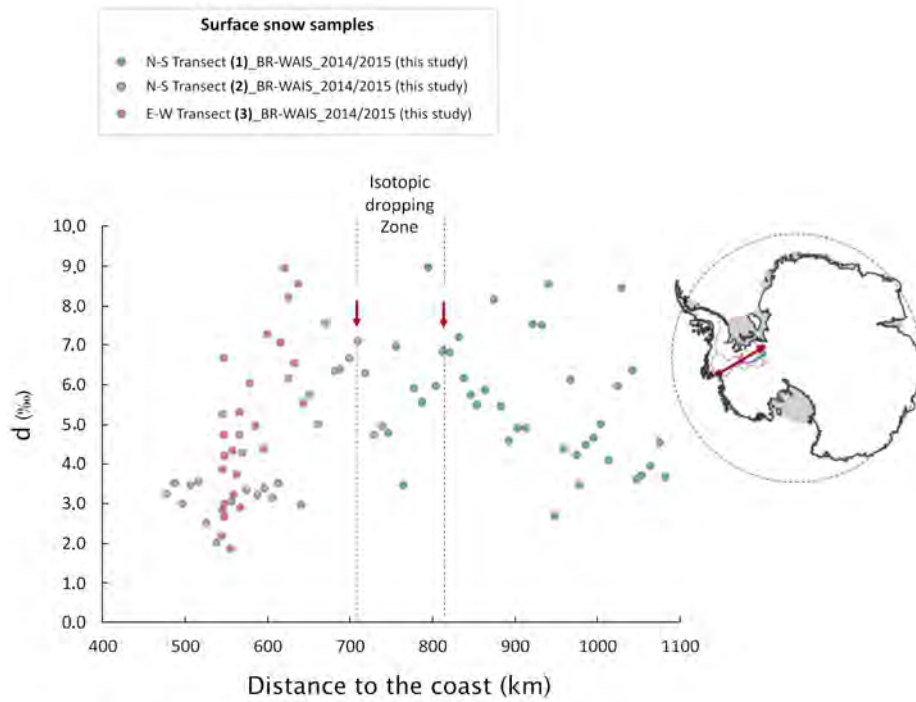
N-S transect (2) and the longitude ( $r = -0.82$ ,  $p < 0.001$ ) in the E-W transect (3) (Table I; Fig. 2a and Fig. 2b). This increase followed roughly up to the same region where the  $\delta s$  signal changed. After that, it tended to decrease slightly toward the south (weak negative correlation with the latitude and distance to the coast ( $r = -0.35$ ;  $p = 0.01-0.05$ ; for both parameters) in the N-S transect (1); Table I). Remarkably, both  $\delta s$  and d-excess behaved randomly in the southernmost part of the N-S transect (1) (around the MIS basin; Fig. 2a). We also identified a well-marked dropping zone in the d-excess signal from 700 to 800 km, S43 and S31, respectively, beyond the PIG ice divide (approximately  $82^\circ$  and  $81^\circ$ S; Fig. 3).

Figure 4 compares our study's  $\delta D$ - $\delta^{18}O$  relations with the global meteoric water line (GMWL; defined by Craig 1961) and the Antarctic Ice Sheet line (AISL; Masson-Delmotte et al. 2008). Our traverse  $\delta D/\delta^{18}O$  line had a slope of  $7.64 \pm 0.07 \text{‰‰}^{-1}$  ( $R^2 = 0.99$ ), and its intercept was  $-9.04 \pm 2.76 \text{‰}$ . Regarding the relationships between d-excess and  $\delta s$ , the former decreased

as the latter increased in the N-S (2) and E-W (3) transects, with d-excess/ $\delta^{18}O$  slopes of  $-0.46 \pm 0.08 \text{‰‰}^{-1}$  ( $R^2 = 0.54$ ) and  $-0.56 \pm 0.15 \text{‰‰}^{-1}$  ( $R^2 = 0.37$ ), respectively (see Table I; Fig. 5c). For the N-S transect (1), there was no linear correlation between  $\delta s$  and d-excess (Table I; Fig. 5b). We compared our d-excess and  $\delta^{18}O$  data with isotopic data from the 1990 International Trans-Antarctica Expedition (ITAE; Dahe et al. 1994) and from the 2014 and 2015 Union Glacier field campaigns (hereafter, UGC; Hoffmann et al. 2020) in the Ellsworth Mountains region (only with the 2014 isotopic data of the PASO-1 ( $79^\circ 38' 00.68''$ S,  $85^\circ 00' 22.51''$ W), BAL-1 ( $79^\circ 31' 27.69''$ S,  $84^\circ 26' 32.09''$ W), SCH-1 ( $79^\circ 31' 14.02''$ S,  $84^\circ 08' 56.48''$ W), GUPA-1 ( $79^\circ 46' 07.00''$ S,  $82^\circ 54' 33.44''$ W) and DOTT-1 ( $79^\circ 18' 38.84''$ S,  $81^\circ 39' 09.33''$ W) firn cores) (Fig. 5). The data used from the ITAE are listed in Table SV. The 2014 isotopic data of the UGC firn cores were extracted from the PANGAEA database (available at: <https://doi.pangaea.de/10.1594/PANGAEA.908205>; Hoffmann et al. 2019).



**Figure 2.** Water stable isotope ratios ( $\delta^{18}O$ ,  $\delta D$ , and d-excess) spatial variation along the N-S (a) and the E-W (b) transects. Blue stars indicate the intersection of the N-S with the E-W transect.



**Figure 3.** Variability of the *d*-excess as a function of the distance from the coast (direction is marked on the map by the red arrow) along the 2015 BR-WAIS traverse route. On the left of the graph, the results for N-S transect (2) (purple dots) and E-W transect (3) (pink dots) results. On the right, the results for N-S transect (1) (green dots).

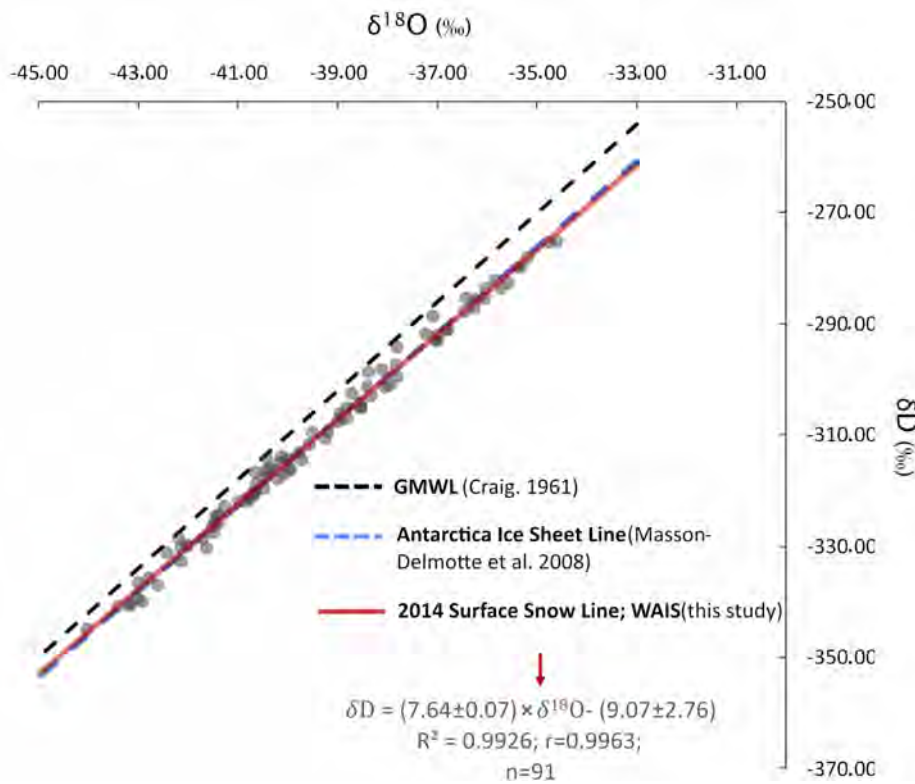


**Figure 4.** Relationship between  $\delta^{18}\text{O}$  and  $\delta\text{D}$  along the 2015 Brazilian traverse route. Gray dots are data from the surface snow samples.

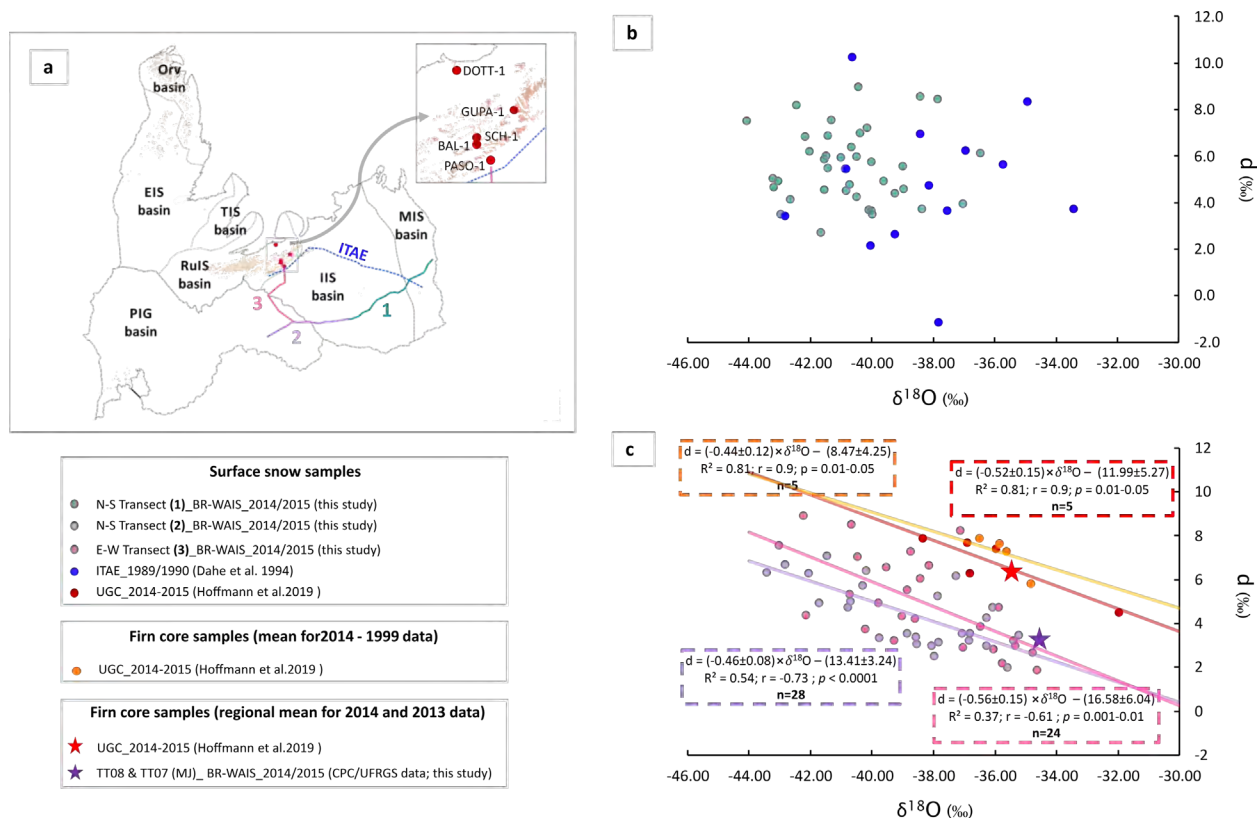


**Figure 5.** Relationship between  $\delta^{18}O$  and  $d$ -excess along the 2015 Brazilian traverse route, 1990 International Trans-Antarctica Expedition (ITAE) route, and the 2014-2015 Union Glacier field campaigns region (UGC). (a) Map showing the location of the transects. For ITAE, only the 13 samples [from sample 38 (79°10' S; 86°51' W) to sample 50 (85°53' S; 88°10' W)] were considered (blue line). For the UGC, only five cores (DOTT-1, GUPA-1, SCH-1, BAL-1, and PASO-1) were considered (red dots). (b)  $d$ - excess/ $\delta^{18}O$  relationship for the N-S transect (1) (green dots) and ITAE route (blue dots). (c)  $d$ -excess/ $\delta^{18}O$  relationship for the N-S transect (2) (purple dots), N-S transect (3) (pink dots), and UGC sites (red dots: plot of 2014 isotopic mean for each firn core; orange dots: plot of 2014-1999 isotopic mean for each firn core). Stars represent 2014-2013 regional mean for the upstream area of the PIG basin (purple: isotopic data from the TT08 (S58 position) and TT07 (S57 position) firn cores) and for the Ellsworth Mountains region (red: isotopic data from UGC firn cores).

### Troposphere temperature cross-sections and seasonal snow precipitation distribution

Figure 6 shows the vertical temperature profile from the surface to a height of 10,000 m along the route of the BR-WAIS traverse. In the N-S transect, it is evident that the ABS sector of the cross-section (PIG basin) was relatively warmer than the WS sector (MIS and IIS basins) in 2014. However, the E-W transect (3) showed a different pattern. In the latter, the temperature was relatively more consistent throughout the

topography, showing a slight increase moving toward the PIG basin.

The annual distribution of snow precipitation for the 11 sites is shown in Figure 7. The 2014 total precipitation (tp) data show that the highest precipitation occurred in the autumn months (MAM) (except for the S30 region), followed by the winter months JJA (except for the S92 region; Table SVI). The summer months (JFM) were the driest at all sites, and the precipitation was slightly higher in the S92, S20, S30, and S40

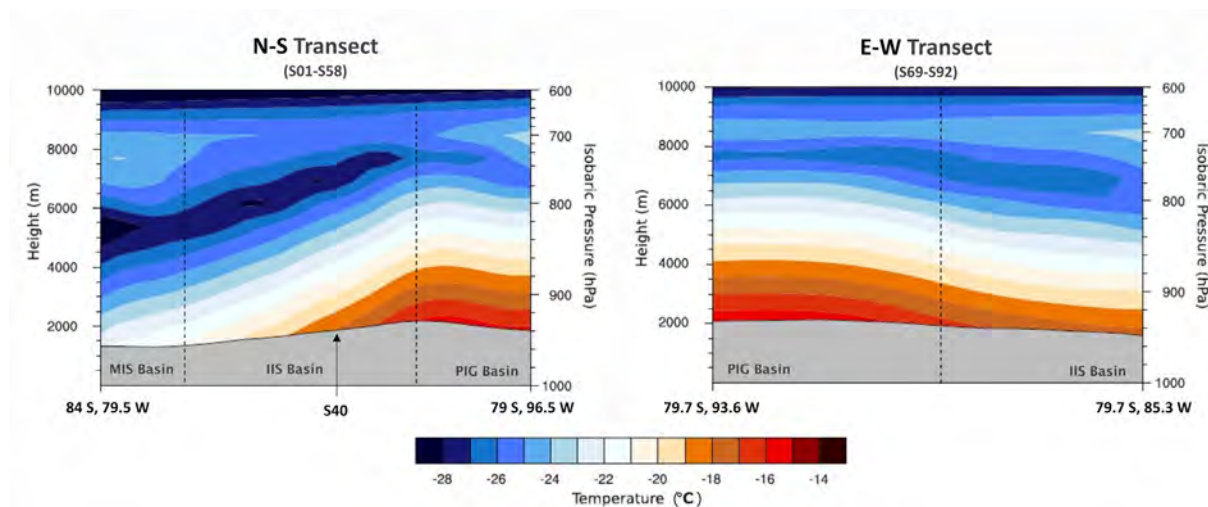


**Figure 6.** Annual mean temperature of the troposphere along the 2014 N-S (on the left) and E-W (on the right) transects. Temperature per height data were extracted from ERA 5 datasets. We emphasize that these temperatures can be interpreted only in relative terms.

regions than in other sites during this season (Table SVI, Fig. 7). Notably, the WS sector was relatively drier ( $tp < 0.19$  m) than the ABS sector ( $tp \geq 0.19$  m) (Table SII). Furthermore, well-marked differences along the route of the BR-WAIS traverse were observed in the 2014 snow precipitation distribution pattern. From S01 to S40 (region of the MIS and IIS basins), April, May, June, July, August, and October were relatively wet. September had more precipitation than July in the region between S50, S58, and S80 (i.e. in the PIG basin region, including the WAIS summit area). Regarding the S92 region (near the Ellsworth Mountains), the highest precipitation occurred in March, April, May, June, July, and October (Fig. 7).

The ERA5 precipitation data agree with similar data from the Antarctic Mesoscale Prediction System (AMPS) archived forecasts of a previous study (Nicolas & Bromwich 2009) performed for the ABS and WS sectors (2006–2007). Additionally, it agrees with regional climate model studies (van Lipzig et al. 2002, Monaghan et al. 2006, Van de Berg et al. 2006) that suggest that most of the annual precipitation in Antarctica occurs in the

autumn (MAM). This agreement allows the use of these data to help interpret the isotopic records.

### Air-masses trajectories

Table II shows the frequencies and origins of the oceanic and continental air masses during the wet and dry seasons. Clustered back trajectories by season for the four sites in the WAIS (S01, S40, S58, and S92) are displayed in Fig. 8 (for the other sites, see Fig. S2). We distinguished the mean trajectories of air masses coming from the ocean with no or negligible sea ice cover from others to capture the potential oceanic areas that primarily contributed to moisture input onto the WAIS in 2014 and verified the contribution differences between the ABS and WS sectors. The air masses from the eastern sector inner part (hereafter, EA sector) originating on sea ice (or near the ocean-sea ice edge) or coming from long distances and traveling much of the time over sea ice were considered continental air masses. Likewise, air masses that entered the continent by the eastern region of the Weddell Sea (Coats Land and Dronning Maud Land) were also considered continental because they

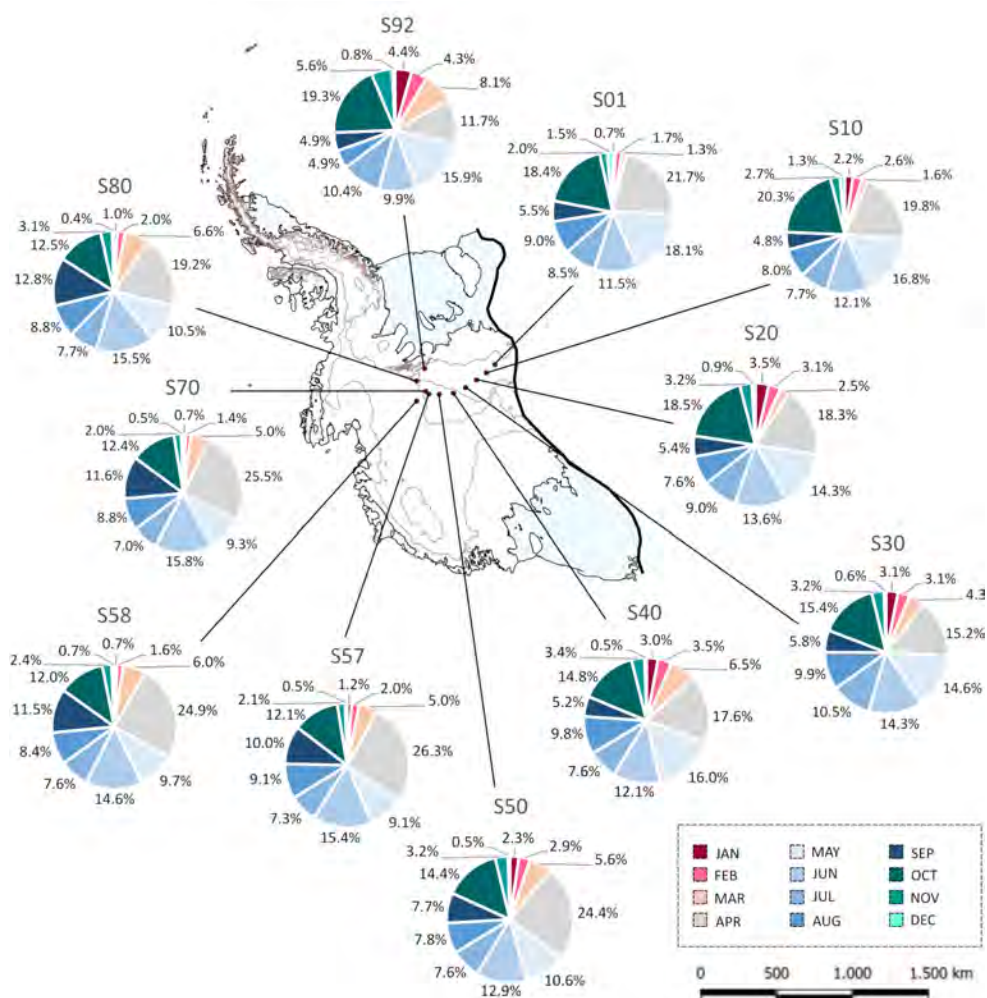


**Figure 7.** Annual distribution (in percentage) of 2014 snow precipitation for eleven sites sampled along the BR-WAIS traverse route. Total precipitation data were extracted from ERA 5 datasets.

interacted with the relatively colder and driest air from the EAIS before arriving in the inner part of the MIS and IIS basins. Figure S3 provides more details regarding the classification.

The 2014 frequency distributions of the clusters (Table II, Fig. 8) indicate that the oceanic influence in the MIS basin and southernmost part of the IIS basin came mainly from the ABS and RS sectors, considering both the wet and dry seasons. On the other hand, the impact of the oceanic air masses on the ABS sector became minor, and the contribution of maritime air masses from the RS and EA sectors increased toward the PIG basin. This increase was more

pronounced during the wet season. Regarding continental influence, the air masses from the WS sector were more critical for the WAIS in the dry season. This influence was strong in the MIS and southernmost part of the IIS basin and minimal toward the PIG basin. Remarkably, in the wet season, the oceanic influence decreased gradually toward the WS sector. This decrease was more pronounced from the PIG (S58) to the inner region of the MIS-IIS basins (S01-S30) than from the PIG to the Ellsworth Mountain region (S92) (Fig. 9). During the dry season, although the oceanic influence was slightly more prominent on the WAIS divide summit than in other

**Table II.** Frequencies (in percentage) and origin of the oceanic and continental backward air masses trajectories clusters for wet (March–August) and dry (January–February and September–December) seasons.

	OCEANIC AIR MASSES			CONTINENTAL AIR MASSES			
	Amundsen-Bellingshausen sector	Ross sector	Eastern sector	Eastern sector*	Weddell sector	Plateau	WAIS
S01							
Wet	17%	7%	-	28%	24%	-	24%
Dry	19%	6%	-	-	46%	27%	-
S10							
Wet	17%	23%	-	36%	12%	-	11%
Dry	20%	6%	-	5%	40%	11%	18%
S20							
Wet	15%	16%	-	13%	10%	20%	27%
Dry	17%	-	-	27%	48%	7%	-
S30							
Wet	12%	21%	18%	14%	18%	16%	-
Dry	25%	14%	-	8%	15%	37%	-
S40							
Wet	14%	16%	15%	25%	-	-	21%
Dry	13%	19%	-	34%	21%	-	13%
S50							
Wet	23%	10%	23%	15%	-	19%	11%
Dry	25%	23%	-	16%	11%	9%	15%
S58							
Wet	13%	35%	21%	10%	10%	-	11%
Dry	11%	15%	-	14%	18%	24%	18%
S70							
Wet	14%	23%	20%	20%	-	-	23%
Dry	13%	26%	-	27%	16%	-	17%
S80							
Wet	22%	12%	20%	14%	-	9%	23%
Dry	16%	22%	-	27%	29%	7%	-
S92							
Wet	18%	27%	13%	16%	8%	18%	-
Dry	19%	9%	-	28%	17%	8%	19%

\*More inner trajectories from the eastern sector.

regions, the presence of continental air masses was dominant throughout the entire BR-WAIS route (Fig. S4; ). Furthermore, the transition zone between oceanic and continental conditions was

approximately between S30 and S50 during the wet season (Fig. 9). The S50 region was equally under oceanic and continental influence during the wet and dry seasons (Fig. 9, Fig. S4).

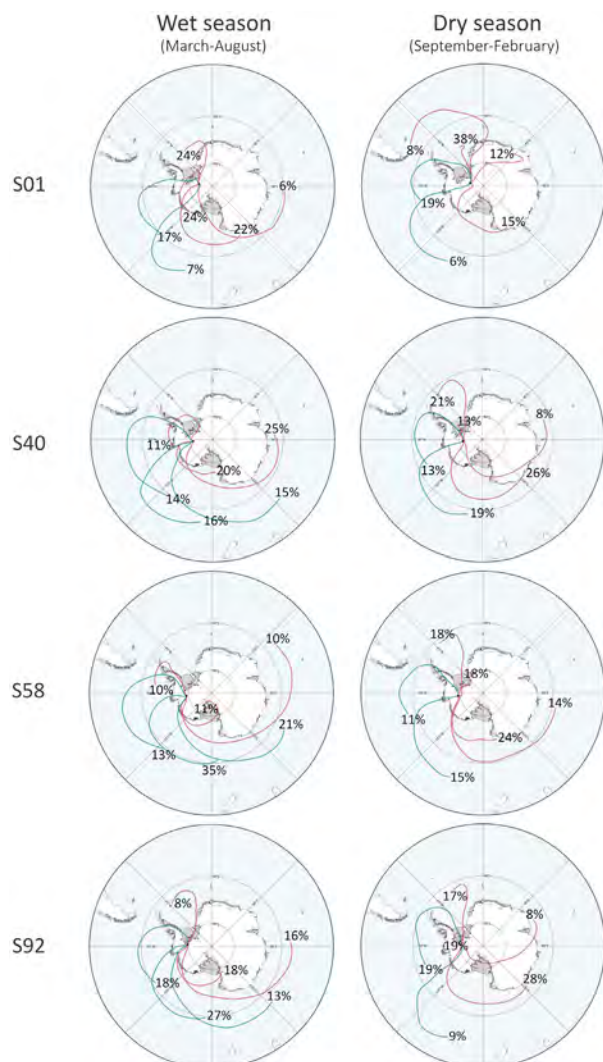


**Figure 8.** Air mass backward trajectory cluster analysis (10-days) by season: air-mass flow pattern for four sites in West Antarctica (S01, S40, S58, and S92) throughout 2014. The percentage of daily trajectories included in each cluster is indicated. The blue clusters represent oceanic air masses, and the pink ones are continental air masses. Trajectories and cluster analysis were performed using the NOAA HYSPLIT model (version 4.9) in conjunction with the NCEP/NCAR atmospheric reanalysis. Results were exported in Shapefile format. The base map is made in QGIS using the Quantarctica 3 Project datasets (Matsuoka et al. 2018).

## DISCUSSION

The first two subsections discuss the spatial distribution of  $\delta_s$  and d-excess, and the third addresses the co-isotopic relationships. In our

study, we also considered the influence of post-depositional processes on the local scale due to fieldwork observations and isotopic data from some parts of the traverse (fourth subsection). The meteorological information (troposphere temperature, snowfall, and air mass movement) is discussed in an integrated way in the previously listed subsections. In the last subsection (fifth), we summarize some points that show the climatic value of the isotopic signal of the BR-WAIS region, address some limitations of our study, and make recommendations for future work.

### Spatial distribution of $\delta^{18}\text{O}$ and $\delta\text{D}$ in the MIS, IIS, and PIG Basins

Our findings for the northernmost part of the IIS and PIG basins (N-S transect (2): S58- S40) revealed a remarkable increase in  $\delta_s$  toward the PIG basin (Fig. 2a). Considering the temperature and intermittency effect on the water isotope ratios, this increase could strongly indicate warmer 2014 precipitation events in the upper reaches of the PIG drainage basin (ABS sector) than those that occurred in the IIS and MIS basins (WS sector). Although we did not model the temperature for precipitation days, this hypothesis could be supported by the troposphere annual mean temperature data (Fig. 6), which show the presence of a warm (oceanic) air mass on the WAIS divide and the ABS sector, indicating that relatively warmer conditions prevailed in 2014 in this region compared to the WS sector.

As this increase in  $\delta_s$  from the northernmost part of the IIS to the PIG is better described by the negative  $\delta_s$ -latitude correlation (and the continentality concerning the PIG coast – ABS sector; Fig. 2a, Table I), it is evident that the preferential air mass distillation path is from the ABS sector coast toward the PIG-IIS ice divide. Moreover, the strong negative correlation

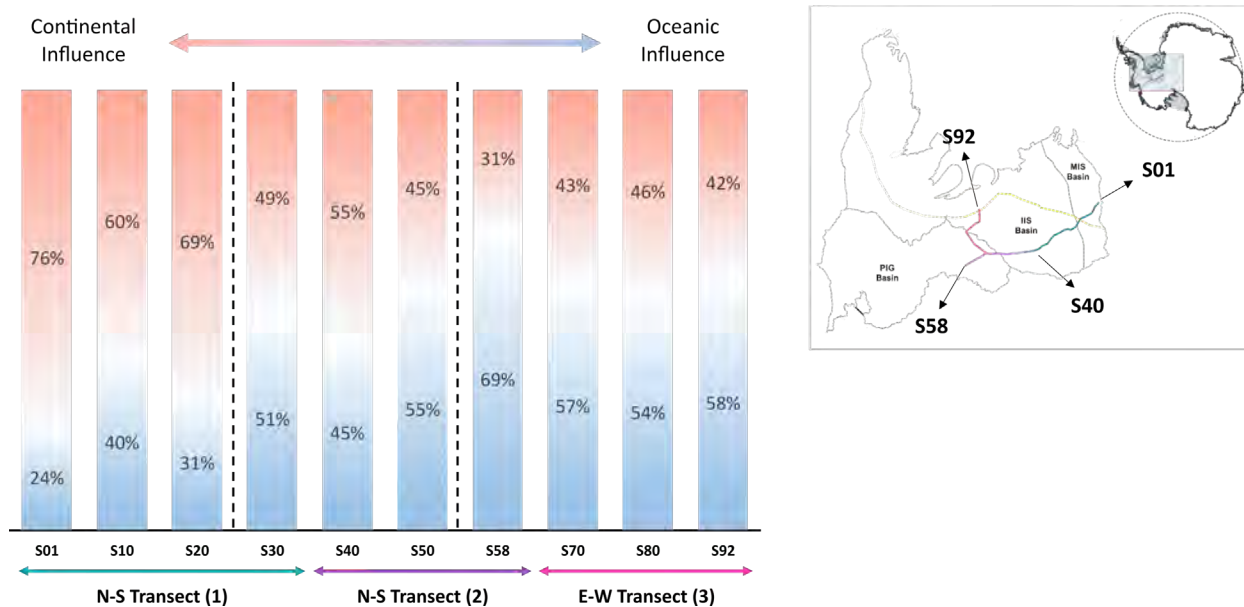


**Figure 9.** Total contribution of the oceanic and continental air masses (in percentage) for the wet season (March–August 2014) along the BR-WAIS traverse route. The percentage was computed by the sum of the clusters of similar nature (i.e., oceanic or continental). The map (on the right) shows the location of the three transects (N-S transect (1), N-S transect (2), and E-W transect (3)) and some samples (S01, S40, S58, S92). Note a transition zone between the S30 and S50 (marked by the dashed lines).

of  $\delta_s$  with distance to the PIG coast may indicate that the isotopic signal is more biased by the moisture-rich cyclones and storm systems penetrating the WAIS by the Amundsen coast than by the Bellingshausen and Peninsula sectors. The air mass simulation results for the wet season corroborate this hypothesis, as shown in Figure 8 and Table II the major influence of the oceanic air masses arriving in the region between S58 and S40 came from the RS and EA sectors.

The negative trends of the isotopic ratios, concerning latitude and continentality, advanced approximately 150 km into the IIS basin (N-S transect (2); Fig. 2a), which may indicate that relatively warmer ocean air masses from the Pacific sector exceed the topographic barrier and contribute to the accumulation of snow in part of the WS sector. In other words, the air masses penetrating the WAIS by the ABS sector continued to cool and move toward the

WS sector, influencing the isotopic signal in this region. Four pieces of evidence support this interpretation: (1) the absence of a significant negative correlation with the altitude (Table I); (2) the dominant northerly transport from the S58 to S40–S50 region during the wet season (mainly from the RS and EA sectors, as previously mentioned; Fig. 8, Table II); (3) the well-marked decrease in the oceanic influence from the S58 region toward the WS sector during the wet season (which in turn is biased by the decrease in the contribution of air masses coming from the EA sector; Fig. 9, Table II); and (4) by the individual  $d$ -excess and  $d$ -excess/ $\delta^{18}\text{O}$  relationship data (discussed below in this article; Fig. 3 and Fig. 5).

The absence of a statistically significant negative  $\delta_s$ -altitude correlation from the PIG to the IIS basin (N-S transect (2); Table I) indicates that the distillation of the air masses from the ABS to the WS sector was mainly controlled by

the temperature decreases toward the WS sector rather than by the altitude effect (reduction of  $\delta s$  as air masses move to higher altitudes). A well-marked temperature gradient (Fig. 6) and the oceanic influence decrease in the interior of the WS sector supports this interpretation (Fig. 9). Even though there was no significant relationship between  $\delta s$ -altitude, this does not mean that the topographic gradient had no control over the air masses' distillation. It has been shown (Masson-Delmotte et al. 2008, Kang et al. 2009, Xiao et al. 2013, Marquette et al. 2015) that in Antarctica (considering segments from the coast to the plateau region), the correlation between  $\delta s$  and altitude is significant and strongly negative (varying between -0.82 and -0.94). Furthermore, a multiple linear regression model (Masson-Delmotte et al. 2008) and a generalized additive model (Wang et al. 2010), using isotopic ratios from polar archives, showed that elevation is the leading geographical factor correlated with the distribution of the stable isotope content in Antarctica. Therefore, given the importance of the altitude effect, we suggest that  $\delta s$ - altitude gradients still need to be better evaluated in this region.

Concerning  $\delta s$  values from the southernmost part of the IIS to MIS basin (N-S transect (1), from samples S39 to S01), there was a zone without an isotopic trend, despite the differences in elevation (~ 800 m) and latitude (~ 2.5°) (Fig. 2a). It is possible that precipitation events in 2014 occurred under a similar temperature regime in this area. Indeed, there is a divergence between latitude and altitude parameters along the N-S transect (1) owing to the WAIS topographical asymmetry. To the best of our knowledge, in the Antarctic region, the latitude (decrease in  $\delta s$  as air masses advance to higher latitudes) and altitude effects are intrinsically related to the decrease in condensation temperature (Dansgaard 1964, Dansgaard et al. 1973, Gat 1996,

confirmed by Masson-Delmotte et al. 2008 and revised by Hou et al. 2013). Another possible explanation is the trajectory effect of the oceanic air masses that advanced into the WS sector. As verified by the air mass simulations in the wet season, there is a comparable influence coming from the RS sector (that overcomes the WAIS divide) and the ABS sector (that enters the continent through the Peninsula region) between the S10 and S20 regions in the wet season (i.e., almost equal influence in most of the N-S transect (1); Fig. 8, Table II). Furthermore, in the dry season, the oceanic contribution from the ABS sector is similar and predominates over the RS sector contribution throughout the entire N-S transect (1) region (MIS basin and the southernmost part of the IIS basin; Table II; Fig. 8 and Fig. S2). In short, the absence of a trend in this region can be explained by the two preferential fractionation paths.

Because the isotopic values of the N-S transect (1) are more continental (predominantly  $\leq -40$  ‰ for  $\delta^{18}\text{O}$  and  $\leq -320$  ‰ for  $\delta\text{D}$ ), and based on the 2014 tropospheric mean temperature (the lowest atmospheric temperature in the MIS basin and the southernmost part of the IIS basin; Fig. 6), we concluded that the isotopic composition along this transect is strongly controlled by the colder air masses prevailing in this sector. The air mass transport pattern also supports this hypothesis, as it is clear that the continental influence in the MIS and IIS (southernmost part) basin regions in the wet and dry seasons (Fig. 8 and Fig. 9) could weaken and strongly alter any moisture input coming from the ocean, which leads to precipitation in the upper reaches of the WS sector with lower  $\delta s$  than in the upper reaches of the PIG basin (ABS sector). Indeed, the presence of colder, denser, and more stable air masses almost all year is a remarkable characteristic of the WS sector (Schwerdtfeger 1975).

The  $\delta s$  trend observed from the WAIS divide (PIG basin) to the Ellsworth Mountains region (E-W transect (3): S69-S92), given by the  $\delta s$ -longitude and  $\delta s$ -altitude relationships (both moderate positive correlations), may be a result of the small condensation temperature difference between the two regions. Two facts corroborate this assumption: first, the  $\delta s$ -altitude relationships have opposite behaviors to the altitude effect proposed by Dansgaard (1964). Second, there was a slight temperature increase toward the PIG basin (Fig. 6). Our data closest to the Ellsworth Mountains ( $-38.81\text{‰}$  for  $\delta^{18}\text{O}$ ,  $-304.99\text{‰}$  for  $\delta\text{D}$ ; S92 position:  $79^{\circ}38'58.0''$  S,  $85^{\circ}18'09.0''$  W) agree with the PASO-1 ice core ( $-38.32\text{‰}$  for  $\delta^{18}\text{O}$ (2014 mean),  $-298.68\text{‰}$  for  $\delta\text{D}$ (2014 mean);  $79^{\circ}38'00.68''$  S,  $85^{\circ}00'22.51''$  W; approximately 6.20 km east of the S92 sample; calculated with data from Hoffmann et al. 2019), which records for 2014 one of the lowest  $\delta$  value within 44 years (in turn, this also supports the hypothesis that precipitation events occurred in this area at a lower temperature than to the PIG area). Hoffmann et al. (2020) pointed out that snow redistribution plays an important role in the Union Glacier region due to katabatic winds. The lack of AWS in the PIG-UG divide (or PIG-IIS divide) makes it impossible to access the local superficial wind speed variation in 2014. However, it is known that the katabatic winds are not as strong in the PASO-1 and S92 region and along the PIG-IIS divide (Parish and Bromwich 2007). In addition, there is evidence of a continentality effect (concerning the Ronne coast, WS sector; Fig. S5) in the Ellsworth region given by:  $\delta^{18}\text{O}(2014) = -0.0822(\pm 0.0026) \times \text{Dist.} + 26.1610(\pm 1.9957)$  ( $R^2=0.99$ ;  $p<0.001$ );  $\delta\text{D}(2014) = -0.6138(\pm 0.0307) \times \text{Dist.} + 182.9600(\pm 23.2548)$  ( $R^2=0.99$ ;  $p<0.001$ ) (obtained with data from Hoffmann et al. 2019).

As in the N-S transect (2), the  $\delta s$  trend from the PIG basin to the Ellsworth Mountains mirrors

the (slight) decrease in the oceanic influence toward the Ellsworth Mountains during the wet season (Fig. 9). Furthermore, the  $\delta s$  trend is also more biased by storms penetrating the WAIS by the Amundsen coast. However, the region of the E- W transect (3) received a few more influences from the air masses originating from the Bellingshausen Sea than did the N-S Transect (2) region. The observation of the continentality effect from the Ronne coast to the Ellsworth region (as previously mentioned), as well as of higher snowfall near the Ellsworth Mountains region, compared to other places in the 2015 BR-WAIS traverse region, in the dry season (Fig. 7; Table SVI) reaffirms this inference mentioned above. Although our air mass parcel simulations did not show significant contribution differences of the air masses coming from the ABS sector between the E-W transect (3) and the N-S transect (2) regions, it is known that the mean longitude position of the ASL shifts eastward in the spring and summer months (Hosking et al. 2013, Raphael et al. 2016), which might have enhanced the migration of the storms that entered the continent through the Peninsula region (or by the western side of the Weddell Sea) toward the interior of the WS sector during this period.

### ***Spatial distribution of d-excess in the MIS, IIS, and PIG Basins***

The d-excess is an essential second-order isotopic parameter for obtaining further climatic information and supporting the interpretation of  $\delta s$  (Hou et al. 2013). Compared to  $\delta s$ , its spatial distribution is poorly documented and understood (Masson-Delmotte et al. 2008, Goursaud et al. 2019). The d-excess reflects water phase changes under non-equilibrium conditions (or kinetic effects). It is a signature of the oceanic moisture source because it depends mostly on the conditions in the evaporative area,

primarily sea surface temperature and relative humidity, and secondarily on the presence of sea ice and wind velocity (Merlivat & Jouzel 1979, Johnsen et al. 1989, Uemura et al. 2012, Kurita 2011, Pfahl & Sodemann 2014, Bonne et al. 2019).

In coastal Antarctica (< 2000 m of altitude), d-excess preserves information about moisture sources (Touzeau et al. 2016, Landais et al. 2017), and its spatial distribution reflects the variety of trajectories (Landais et al. 2017) because of the strong influence of cyclonic activity around the continent (Simmonds et al. 2003). In the interior of Antarctica (> 2000 m in altitude), d-excess is more sensitive to condensation temperature (it correlates negatively with temperature) because of changes in equilibrium coefficients and ice crystal formation under supersaturation conditions (kinetic fractionation) as a result of the low-temperature conditions (Jouzel & Merlivat 1984, Vimeux et al. 1999, Masson-Delmotte et al. 2008, Touzeau et al. 2016, Landais et al. 2017). Such sensitivity explains the evidence of more significant correlations with geographical features (moderate and positive correlations) (Masson-Delmotte et al. 2008, Hou et al. 2013).

The d-excess data from the BR-WAIS traverse reflect both the trajectory and temperature influence. The slight increase in the d-excess from Criosfera 1 to the ABS sector (marked by the  $\delta s$ -longitude) is also indicative of a preferential distillation path from the eastern side of the Antarctic Peninsula (WS sector) to the Weddell-Ross divide in the IIS-MIS basin region (as previously discussed). In addition, this trend highlights the higher sensitivity of d-excess to the orographic gradient compared to  $\delta s$ . Regarding the trends observed for d-excess along the transects N-S (2) and E-W (3) (Fig. 3), they also agree with the interpretations of  $\delta s$ : they mark a preferential fractionation path from the ABS to WS sector and the influence of the

relatively warm air masses coming from the Pacific sector over the Weddell sector.

Furthermore, the d-excess observed in the traverse region highlights its great susceptibility for post-depositional (discussed later in this article) and depositional (referring to the isotopic dropping zone between 81 and 82 °S) processes. Concerning the latter, the slight increase in  $\delta s$  and expressive reduction in d-excess could result from sublimation, as heavy isotopes are preferably left in the solid phase (Neumann et al. 2008). However, it is challenging to explain the existence of an expressive sublimation zone restricted to ~100 km in an area (IIS-RS divide) that is less affected by strong katabatic winds (Parish and Bromwich 2007). Although the sublimation occurs broadly throughout the WAIS (Lenaerts & van den Broeke 2012), in the upstream areas of the IIS and PIG basins, it does not exceed 10% of the annual surface snow (Bromwich et al. 2004, Lenaerts & van den Broeke 2012). Furthermore, a similar isotopic pattern has been reported in other mountainous areas, and this phenomenon has been called the “inverse altitude effect” (Jiao et al. 2019). This inverse effect is a result of a complex interaction between moisture sources on the slope of the mountains (not far from the summit); however, its mechanism is not yet fully understood.

### Co-isotopic relationships

The  $\delta D$ - $\delta^{18}O$  spatial co-isotopic relationship slope ( $7.64 \pm 0.07 \text{ ‰ ‰}^{-1}$ ) obtained from the BR-WAIS traverse is close to AISL ( $7.75 \pm 0.02 \text{ ‰ ‰}^{-1}$ ) and overlaps the UGCL2014 [described by  $\delta D = 7.48 (\pm 0.15) \times \delta^{18}O - 11.97 (\pm 5.29)$ ;  $R^2 = 0.99$  and  $n = 5$  (computed with 2014 mean isotopic data of the DOTT-1, GUPA-1, SCH-1, BAL-1, and PASO-1; Hoffmann et al. 2019)]. Moreover, it is also close to the results from other surface snow studies in parts of East Antarctica:  $7.5 \pm 0.1 \text{ ‰ ‰}^{-1}$  (Xiao

et al. 2013), 7.85 ‰ ‰<sup>-1</sup> (Kanget al. 2009), and 7.78 ‰ ‰<sup>-1</sup> (for surface snow (1 m) recovered from the Antarctica Peninsula to the Mirny Station (66°33.2'S, 93°00.6'E, East Antarctica; ITAE, Dahe et al. 1994)). These proximities are important because they ensure the reliability of our data.

Water stable isotopes are integrated tracers of the hydrological water cycle (Jouzel 2013), that is, they imprint the conditions in the moisture source area and each process (evaporation, condensation, mixing, atmospheric transport mechanism, sublimation) that occurs along the moisture path and after the deposition, both under equilibrium and non-equilibrium conditions. The spatial co-isotopic relationship between water isotope compositions can be understood as a hydrological fingerprint of a region or glacial drainage basin in Antarctica. With this in mind, we argue that these relationships mark differences between the ABS and WS sectors in terms of the moisture origin, the history of fractionation in the atmosphere, and post-depositional processes, reinforcing what was verified by evaluating individual signals of the  $\delta s$  and d-excess.

The d-excess/ $\delta s$  negative correlation (Fig. 5c; Table I) may indicate that an intense air mass distillation could occur when the air masses coming from the Pacific Sector advance into the interior of the IIS basin (WS sector). This is supported by the 2014 tropospheric temperature profiles (Fig. 6), which indicate that the temperature contrasts between the ABS and WS sectors (IIS and MIS basins) occur throughout the year. The differences between d-excess- $\delta s$  spatial relationships obtained for the upper reaches of the PIG basin region and Ellsworth Mountains region may mark the two preferred fractionation paths observed in the BR-WAIS Traverse region (previously discussed). Although the error obtained in the linear model is considerable, the regional mean data of the

$\delta^{18}O$  and d-excess from the PIG (computed by the 2014-2013 data from the TT08 and TT07 (MJ)) and Ellsworth region (computed by the 2014-2013 data from the DOTT-1, GUPA-1, SCH-1, BAL-1, and PASO-1) could support this interpretation. In addition, the plot of the  $\delta^{18}O$  and d-excess for the N-S Transect (1) and ITAE data (Fig. 5b; Table I) seems to reflect these two preferential isotopic trends observed in Fig. 5c. Therefore, the absence of the d-excess- $\delta s$  correlation in the interior of the WS sector could be the result of the more extensive variety of moisture sources that this sector receives, both from the oceanic (as previously mentioned) and local (blowing and drifting snow contribution; discussed in the following subsection) origins.

### Post-depositional process

The isotopic composition oscillated vigorously in the MIS Basin (Fig. 2a). Based on field observations, we interpreted this as a result of the sastrugi fields in this area. Indeed, this region is a confluence zone of katabatic winds blowing downslope from the Antarctic Plateau due to the terrain configuration (orientation and gradient) (Parish and Bromwich 2007). Therefore, post-depositional features formed by winds and phenomena driven by winds (e.g., snow blowing and drifting snow) are common in this region. For instance, wind-driven sublimation could affect up to ~20% of the annual surface snow in the MIS basin region on days with extreme wind speeds (Bromwich et al 2004, Lenaerts & van den Broeke 2012). In addition to the removal and deposition of snow blown by the wind, a mechanism analogous to that described in the Kohnen station region (Atlantic sector of the EAIS; Ritter et al. 2016) and also on the Dumont d'Urville coast (Pacific sector of the EAIS; Bréant et al. 2019) can be expected to occur in the WS sector: in periods of strong katabatic winds, the relatively dry air masses with low  $\delta s$  and high

d-excess advected from the Antarctic Plateau may affect the isotopic composition of the snow by exchanges on the surface.

However, our  $\delta s$  values were within the modeled range for this region (see Wang et al. 2010 and Hou et al. 2013). The d-excess data for S01 (3.6 ‰) and S02 (4.5 ‰) were close to the mean d-excess in an ice core drilled at the Criosfera 1 site (d-excess mean for  $16 \pm 1$  years (2000–2014): 4.5 ‰; unpublished data from the CPC/UFRGS). Further, the d-excess values also tended to decrease from the IIS basin to the MIS basin (as previously mentioned). Taking into consideration these observations, we concluded that: (1) our annual isotopic signal in snow samples mirrored the local d-excess signature at the Criosfera 1 site; (2) the sites where the d-excess values were far from the general trend were the ones that, possibly, were most affected by the katabatic winds. Nonetheless, further studies are needed to understand how much the aforementioned post-depositional processes affect the isotopic composition in the MIS basin (i.e., the hydrological cycle in the MIS basin region still needs to be clarified).

### **Climatic value, limitations, and recommendations for future works**

The analysis of all  $\delta s$  trends and meteorological information from the three transects of the 2015 BR-WAIS traverse produced two relevant observations: 1) The area where the isotopic trend signal changed in the N-S transect nearly coincided with the area where the warmer air mass wedge terminated (as observed in the troposphere temperature profile), with the change in the annual snow distribution pattern, and with the transition zone of influence from oceanic to continental air masses in the wet season. This coincidence indicated that the annual isotopic signal was sensitive to the known climatic asymmetry between the two sectors.

2) The moisture that arrived in the BR-WAIS traverse region came predominantly from the Pacific Sector, mainly from around 50°S (area over the Pacific Ocean where evaporation is substantial in the winter months, as modeled by Sodemann and Stohl, 2009). Furthermore, the spatial distribution of the water stable isotope composition (based on their annual mean) in the BR-WAIS traverse region reflected the dominant transport path of these oceanic air masses from the Pacific sector during the wet season. Thus, it is assumed that any significant change in the Pacific Ocean and the ASL climatological zone may be reflected in the isotopic composition of the precipitation in the BR-WAIS traverse region (especially changes that lead to significant variations in the sea ice cover in the ABS sector).

We worked with annual means; thus, many individual events and depositional and post-depositional (local) processes were inaccessible for evaluation. Furthermore, we could not assess the seasonal variability of the water stable isotope compositions at all sampled sites. We assumed that the collected surface snow areas faithfully represented the 2014 precipitation events (or at least the most significant snowfall events that, in fact, weighed on the isotopic composition of each sampled site). Finally, we could not discard the possibility of katabatic winds' substantial influence on the isotopic signal of the WS sector, especially in the MIS basin. Thus, future work is necessary to assess whether the ice cores collected in the BR-WAIS traverse route record spatial variations of the warm air masses and improve our understanding of the katabatic winds on the MIS basin snow isotopic composition.

### **CONCLUSIONS**

We investigated the air mass preferential fractionation path, moisture sources, and

climatic signal quality preserved in surface snow in the upper parts of the three glacial drainage basins (PIG, IIS, and MIS) by analyzing the stable isotope spatial variability ( $\delta^{18}\text{O}$ ,  $\delta\text{D}$ , and d-excess) and co-isotopic relationships coupled with meteorological information (troposphere mean annual temperature, snow precipitation, and seasonal airflow patterns). Our results suggest that the annual isotopic signal is biased in autumn and winter months. The PIG basin and northernmost part of the IIS basin mainly receive precipitation of air masses that penetrate the continent through the ABS sector. Meanwhile, the IIS (southernmost part) and MIS basins receive precipitation mainly from the oceanic air masses entering the continent through the western side of the WS sector (i.e., by the Antarctic Peninsula) and also from the air masses that enter the continent through the ABS side and overcome the WAIS divide. The Pacific sector is the primary source of moisture that arrives in the BR-WAIS traverse region. Isotopic compositions proved to be good markers of the air masses that influence the climate of this region. The relatively warmer (maritime) air masses are sourced from the Pacific sector and exert a dominant influence on the ABS sector and WAIS divide, while the colder air masses (continental or maritime strongly modified) exert a major influence on the WS sector. Furthermore, isotopic compositions captured the effect of the warm air masses in part of the Weddell sector in a year (2014) when one of the most significant sea ice extensions occurred. Our isotopic results were sensitive to capturing the well-known climatic asymmetry between ABS and WS sectors, not coincident with the physical limit between the two sectors (150 km south of the PIG-IIS ice divide). Challenges concerning post-depositional processes in the MIS basin still need to be better clarified.

## Acknowledgments

Andressa M. de Oliveira thanks the Fundação de Amparo à Pesquisa do Estado do Rio Grande do Sul (FAPERGS) for a scientific initiation scholarship. This work was accomplished with resources from the Conselho Nacional de Desenvolvimento Científico e Tecnológico (CNPq, Process no. 465680/2014-3 - INCT da Criosfera). We thank the support of our colleagues Filipe G. L. Lindau and Luciano Marquetto during the fieldwork.

## REFERENCES

- BELL RE & SEROUSSI H. 2020. History, mass loss, structure, and dynamic behavior of the Antarctic Ice Sheet. *Science* 367(6484): 1321-1325.
- BONNE JL, BEHRENS M, MEYER H, KIPFSTUHL S, RABE B, SCHÖNICKE L, STEEN-LARSEN HC & WERNER M. 2019. Resolving the controls of water vapor isotopes in the Atlantic sector. *Nat Commun* 10(1): 1-10.
- BRÉANT C ET AL. 2019. Coastal water vapor isotopic composition driven by katabatic wind variability in summer at Dumont d'Urville, coastal East Antarctica. *Earth Planet Sci Lett* 514: 37-47.
- BROMWICH DH, NICOLAS JP, MONAGHAN AJ, LAZZARA MA, KELLER LM, WEIDNER GA & WILSON AB. 2013. Central West Antarctica among the most rapidly warming regions on Earth. *Nat Geosci* 6: 139-145.
- BROMWICH DH, GUO Z, BAI L & CHEN Q. 2004. Modeled Antarctic precipitation. Part I: Spatial and Temporal Variability. *J Climate* 17 (3): 427-447.
- COPERNICUS CLIMATE CHANGE SERVICE (C3S). 2017. Fifth generation of ECMWF atmospheric reanalysis of the global climate. Copernicus Climate Change Service. Available at: <https://cds.climate.eu>. Access at: January 2021.
- CRAIG H. 1961. Isotopic variations in meteoric waters. *Science* 133 (3465): 1702-1703.
- DAHE Q, PETIT J, JOUZEL J & STIEVENARD M. 1994. Distribution of stable isotopes in surface snow along the route of the 1990 International Trans-Antarctica Expedition. *J Glaciol* 40(134): 107-118.
- DANSGAARD W. 1954. The oxygen-18 abundance in fresh water. *Geochim Cosmochim Acta* 6: 241-260.
- DANSGAARD W. 1964. Stable isotopes in precipitation. *Tellus A* 16(4): 436-468.
- DANSGAARD W, JOHNSEN SJ, CLAUSEN HB & GUNDESTRUP N. 1973. Stable isotope glaciology. *Medd Grønland* 197(2): 1-53.

- DEE DP ET AL. 2011. The ERA-Interim reanalysis: configuration and performance of the data assimilation system. *Quart J Roy Meteor Soc* 137: 553-597.
- DELAYGUE G, MASSON V, JOUZEL J, KOSTER RD & HEALY RJ. 2000. The origin of Antarctic precipitation: a modelling approach. *Tellus B* 52(1): 19-36.
- DING Q, STEIG EJ, BATTISTI DS & KÜTTEL M. 2011. Winter warming in West Antarctica caused by central tropical Pacific warming. *Nat Geosci* 4(6): 398-403.
- DIXON DA, MAYEWSKI PA, GOODWIN ID, MARSHALL, GJ, FREEMAN R, MAASCH KA & SNEED SB. 2012. An ice-core proxy for northerly air mass incursions into West Antarctica. *Int J Climatol* 32(10): 1455-1465.
- DRAXLER RR & HESS GD. 1998. An overview of the HYSPLIT\_4 modeling system for trajectories, dispersion, and deposition. *Aust Meteor Mag* 4: 295-308.
- EPICA COMMUNITY MEMBERS. 2004. Eight glacial cycles from an Antarctic ice core. *Nature* 429(6992): 623-628.
- EPSTEIN S & MAYEDA T. 1953. Variations of  $O^{18}$  content of waters from natural sources. *Geochim Cosmochim Acta* 4(5): 213-224.
- EPSTEIN S, SHARP RP & GODDARD I. 1963. Oxygen isotope ratios in Antarctica snow, firn and ice. *J Geol* 71: 698-720.
- GAT JR. 1996. Oxygen and hydrogen isotopes in the hydrologic cycle. *Annu Rev Earth Planet Sci* 24: 225-262.
- GOURSAUD S, MASSON-DELMOTTE V, FAVIER V, PREUNKERT S, LEGRAND M, MINSTER B & WERNER M. 2019. Challenges associated with the climatic interpretation of water stable isotopes records from a highly resolved firn core from Adélie Land, coastal Antarctica. *The Cryosphere* 13: 1297-1324.
- HERSBACH H ET AL. 2019. Global reanalysis: goodbye ERA-Interim, hello ERA5. *ECMWF newsletter* 159: 17-24.
- HERSBACH H & DEE D. 2016. ERA5 reanalysis is in production. *ECMWF newsletter* 147: 7.
- HOFFMANN K ET AL. 2019. High-resolution stable composition ( $\delta^{18}O$ ,  $\delta D$ ,  $d$  excess) and accumulation rates of six firn cores from Union Glacier, Ellsworth Mountains, West Antarctica, 1973-2014. *PANGAEA*.
- HOFFMANN K ET AL. 2020. Stable water isotopes and accumulation rates in the Union Glacier region, Ellsworth Mountains, West Antarctica, over the last 35 years. *The Cryosphere* 14 (3): 881-904.
- HOSKING JS, ORR A, MARSHALL GJ, TURNER J & PHILLIPS T. 2013. The influence of the Amundsen-Bellinghousen Seas Low on the Climate of West Antarctica and its representation in coupled climate model simulations. *J Clim* 26: 6633-6648.
- HOU SG, WANG YT & PANG HX. 2013. Climatology of stable isotopes in Antarctic snow and ice: Current status and prospects. *Chin Sci Bull* 58(10): 1095-1106.
- JIAO Y, LIU C, GAO X, XU Q, DING Y & LIU Z. 2019. Impacts of moisture sources on the isotopic inverse altitude effect and amount of precipitation in the Hani Rice Terraces region of the Ailao Mountains. *Sci Total Environ* 687: 470-478.
- JOHNSEN SJ, DANSGAARD W, CLAUSEN HB, & LANGWAY CC. 1972. Oxygen isotope profiles through the Antarctic and Greenland ice sheets. *Nature* 235(5339): 429-434.
- JOHNSEN SJ, DANSGAARD W & WHITE JWC. 1989. The origin of Arctic precipitation under present and glacial conditions. *Tellus B* 41(4): 452-468.
- JOUZEL J. 2013. Water Stables Isotopes: Atmospheric Composition and Applications in Polar Ice core Studies. 2<sup>nd</sup> ed., *Treatise on Geochemistry* vol. 5 Elsevier Ltd.
- JOUZEL J ET AL. 2007. Orbital and millennial Antarctic climate variability over the past 800,000 years. *Science* 317: 793-796.
- JOUZEL J & MERLIVAT L. 1984. Deuterium and oxygen 18 in precipitation: Modeling of the isotopic effects during snow formation. *J Geophys Res* 89(D7) 11749-11757.
- KALNAY E ET AL. 1996. The NCEP/NCAR 40-year reanalysis project. *B Am Meteorol Soc* 77: 437-471.
- KANG JC, JOUZEL J, STIEVENARD M, QIN D, LIU L, WANG D, LI Z & LI J. 2009. Variation of stable isotopes in surface snow along a traverse from coast to plateau's interior in East Antarctica and its climatic significance. *Sci Cold Arid Reg* 1(1): 0014-0024.
- KURITA N. 2011. Origin of Arctic water vapor during the ice-growth season. *Geophys Res Lett* 38(2).
- KÜTTEL M, STEIG EJ, DING Q, MONAGHAN AJ & BATTISTI DS. 2012. Seasonal climate information preserved in West Antarctica ice core water isotopes: relationships to temperature, large-scale circulation, and sea ice. *Clim Dyn* 39(7-8): 1841-1857.
- LANDAIS A ET AL. 2017. Surface studies of water isotopes in Antarctica for quantitative interpretation of deep ice core data. *Compt Rend Geosci* 349: 139-150.
- LENAERTS JTM & VAN DEN BROEKE MR. 2012. Modeling drifting snow in Antarctica with a regional climate model: 2. Results. *J Geophys Res* 117 (D05109).

- LINDAU FGL, SIMÕES JC, MARQUES MM, HAMMES DF, DA SILVA DB, CASASSA G, SNEED S & INTRONE D. 2016. Variabilidade do conteúdo iônico da neve e do firn ao longo de um transecto antártico. *Pesq Geoci* 43 (3): 213-228.
- MARKLE BR, BERTLER NAN, SINCLAIR KE & SNEED SB. 2012. Synoptic variability in the Ross Sea region, Antarctica, as seen from back-trajectory modeling and ice core analysis. *J Geophys Res* 117(D2).
- MARQUETTO L, KASPARI, S & SIMÕES JC. 2020. Refractory black carbon (rBC) variability in a 47-year West Antarctic snow and firn core. *The Cryosphere* 14(5): 1537-1554.
- MARQUETTO L, SIMÕES JC, CASASSA G, INTRONE DS & DOS SANTOS EA. 2015. Variações na composição isotópica de oxigênio na neve superficial ao longo de uma travessia antártica. *Pesqui Geoci* 42 (3):227-238.
- MASSON-DELMOTTE V ET AL. 2008. A Review of Antarctic Surface Snow Isotopic Composition: Observations, Atmospheric Circulation, and Isotopic Modeling. *J Clim* 21(13): 3359-3387.
- MATSUOKA K, SKOGLUND A & ROTH G. 2018. Quantarctica. Norwegian Polar Institute. <https://doi.org/10.21334/npolar.2018.8516e961>.
- MAYEWSKI PA. 2006. International Trans-Antarctic Scientific Expedition (ITASE). *Pages News* 14(1): 26-28.
- MAYEWSKI PA & GOODWIN I. 1997. International Trans-Antarctic Scientific Expedition (ITASE) - "200 years of past Antarctic and Environmental Change". Science and Implementation Plan - Report from ITASE Workshop.
- MERLIVAT L & JOUZEL J. 1979. Global climatic interpretation of the deuterium-oxygen 18 relationship for precipitation. *J Geophys Res* 84(C8): 5029-5033.
- MONAGHAN AJ, BROMWICH DH, & WANG, SH. 2006. Recent trends in Antarctic snow accumulation from Polar MM5 simulations. *Philos Trans A Math Phys Eng Sci* 364(1844): 1683-1708.
- NEUMANN TA, ALBERT MR, LOMONACO R, ENGEL C, COURVILLE Z & PERRON F. 2008. Experimental determination of snow sublimation rate and stable- isotopic exchange. *Ann Glaciol* 49: 1-6.
- NICOLAS JP & BROMWICH DH. 2009. Marine signature in West Antarctic climate as seen by AMPS. 10<sup>th</sup> Conference on Polar Meteorology and Oceanography.
- NICOLAS JP & BROMWICH DH. 2011. Climate of West Antarctica and Influence of Marine Air Intrusions. *J Clim* 24 (1): 49-67.
- NOONE D. 2008. The influence of midlatitudes and tropical overturning circulation on the isotopic composition of atmospheric water vapor and Antarctic precipitation. *J Geophys Res* 113 (D4).
- NOONE D & SIMMONDS I. 2002. Annular variations in moisture transport mechanisms and the abundance of d<sup>18</sup>O in Antarctic snow. *J Geophys Res* 107(D24): 4742.
- NOONE D & SIMMONDS I. 2004. Sea ice control of water isotope transport to Antarctica and implications for ice core interpretation. *J Geophys Res* 109 (D7).
- PARISH TR & BROMWICH DH. 2007. Reexamination of the near-surface airflow over the Antarctic continent and implications on atmospheric circulations at high southern latitudes. *Mon Weather Rev* 135(5): 1961-1973.
- PETIT J-R ET AL. 1999. Climate and atmospheric history of the past 420,000 years from Vostok ice core, Antarctica. *Nature* 399(6735): 429-436.
- PETIT J-R, WHITE J, YOUNG N, JOUZEL J & KOROTKEVICH YE S. 1991. Deuterium excess in recent Antarctica snow. *J Geophys Res* 96(D3): 5113-5122.
- PFAHL S & SODEMANN H. 2014. What controls deuterium excess in global precipitation? *Clim Past* 10(2): 771-781.
- PINTO TAA. 2017. Análise estatística dos dados meteorológicos do Criosfera 1 (84°S 079.9°W), entre 2012 e 2017, na Antártica Oeste. Niterói, RJ 86p. Dissertação de mestrado. Programa de Pós Graduação em Engenharia de Biosistemas, Universidade Federal Fluminense. (Unpublished).
- PRITCHARD HD, LIGTENBERG SRM, FRIECKER HA, VAUGHAN DG, VAN DEN BROEKE MR & PADMAN L. 2012. Antarctic ice-sheet loss driven by basal melting of ice shelves. *Nature* 484: 502-505.
- RAPHAEL MN, MARSHALL GJ, TURNER J, FOGT RL, SCHNEIDER D, DIXON DA, HOSKING JS, JONES JM & HOBBS WR. 2016. The Amundsen Sea Low: Variability, Change and Impact on Antarctica Climate. *Bull Am Met Soc* 97(1): 111-121.
- RIGNOT E, BAMBER JL, VAN DEN BROEKE MR, DAVIS C, LI Y, VAN DE BERG WJ & MEIJGAARD EV. 2008. Recent Antarctica ice-mass loss from radar interferometry and regional climate modeling. *Nat Geosci* 1: 106-110.
- RITTER ET AL. 2016. Isotopic exchange on the diurnal scale between near-surface snow and lower atmospheric water vapor at Kohnen station, East Antarctica. *The Cryosphere* 10: 1647-1663.
- SCHNEIDER DP & STEIG EJ. 2008. Ice cores record significant 1940s Antarctic warmth related to tropical climate variability. *PNAS* 105(34): 12154-12158.
- SCHWANK F, SIMÕES JC, HANDLEY M, MAYEWSKI PA, AUGER JD, BERNARDO RT & AQUINO FE. 2017. A 125-year record of

climate and chemistry variability at Pine Island Glacier ice divide, Antarctica. *The Cryosphere* 11: 1537-1552.

SCHWANCK F, SIMÕES JC, HANDLEY M, MAYEWSKI PA, BERNARDO RT & AQUINO FE. 2016. Anomalously high arsenic concentration in a West Antarctic ice core and its relationship to copper mining in Chile. *Atmos Environ* 125: 257-264.

SCHWERDTFEGGER W. 1975. The effect of the Antarctic Peninsula on the temperature regime of the Weddell Sea. *Mon Weather Rev* 103(1): 45-51.

SHEPHERD A, FRICKER HA & FARRELL SL. 2018. Trends and connections across the Antarctic cryosphere. *Nature* 558(7709): 223-232.

SIEGERT MJ ET AL. 2019. Major ice sheet change in the Weddell Sea sector of West Antarctica over the last 5,000 years. *Rev Geophys* 57(4): 1197-1223.

SIMMONDS I, KEAY K & LIM EP. 2003. Synoptic activity in the seas around Antarctica. *Mon Weather Rev* 131(2): 272-288.

SODEMANN H & STOHL A. 2009. Asymmetries in the moisture origin of Antarctic precipitation. *Geophys Res Lett* 36 (22): L22803.

STEIG EJ, SCHNEIDER DP, RUTHERFORD SD, MANN ME, COMISO JC & SHINDELL DT. 2009. Warming of the Antarctic ice-sheet surface since the 1957 International Geophysical Year. *Nature* 457: 459-462.

STEIN AF, DRAXLER RR, ROLPH GD, STUNDER BJB, COHEN MD & NGAN F. 2015. NOAA's HYSPLIT atmospheric transport and dispersion modeling system. *Bull Amer Meteor* 96 (12) 2059-2077.

TETZNER D, THOMAS E & ALLEN C. 2019. A validation of ERA5 Reanalysis Data in Southern Antarctica Peninsula-Ellsworth Land Region, and Its Implication for Ice Core Studies. *Geosciences* 9(7): 289.

TOUZEAU A ET AL. 2016. Acquisition of isotopic composition for surface snow in East Antarctica and the links to climatic parameters. *The Cryosphere* 10: 837-852.

TURNER J. 2009. Antarctic climate change and the environment, 555 p.

TURNER J, LACHLAN-COPE TA, COLWELL S, MARSHALL GJ & CONNOLLEY WM. 2006. Significant Warming of the Antarctica winter Troposphere. *Science* 311(5769): 1914-1917.

TURNER J, LU H, WHITE I, KING JC, PHILLIPS T, HOSKING JS, BRACEGIRDLE TJ, MARSHALL GJ, MULVANEY R & DEB P. 2016. Absence of 21<sup>st</sup> century warming on Antarctic Peninsula consistent with natural variability. *Nature* 535(7612): 411-415.

UEMURA R, MASSON-DELMOTTE V, JOUZEL J, LANDAIS A, MOTOYAMA H & STENNI B. 2012. Ranges of moisture-source temperature estimated from Antarctic ice cores stable isotope records over glacial-interglacial cycles. *Clim Past* 8(3): 1109-1125.

VAN DE BERG WJ, VAN DEN BROEKE MR, REIJMER CH & VAN MEIJGAARD E. 2006. Characteristics of the Antarctic surface mass balance (1958-2002) using a regional atmospheric climate model. *Ann Glaciol* 41: 97-104.

VAN LIPZIG NPM, VAN MEIJGAARD E & OERLEMANS J. 2002. The spatial and temporal variability of the surface mass balance in Antarctica: results from a regional atmospheric climate model. *Int J Climatol* 22: 1197-1217.

VIMEUX F, MASSON V, JOUZEL J, STIEVENARD M & PETIT JR. 1999. Glacial-interglacial changes in ocean surface conditions in the Southern Hemisphere. *Nature* 398(6726): 410-413.

WAIS DIVIDE PROJECT MEMBERS. 2013. Onset of deglacial warming in West Antarctica driven by local orbital forcing. *Nature* 500: 440-444.

WANG Y, HOU S, MASSON-DELMOTTE V & JOUZEL J. 2010. A generalized additive model for spatial distribution of stable isotopic composition in Antarctic surface snow. *Chem Geol* 271: 133-141.

WILLE JD, FAVIER V, DUFOUR A, GORODETSKAYA IV, TURNER J, AGOSTA C & CODRON F. 2019. West Antarctic surface melt triggered by atmospheric rivers. *Nat Geosci* 12(11): 911-916.

XIAO C ET AL. 2013. Stable isotopes in surface snow along a traverse route from Zhongshan station to Dome A, East Antarctica. *Clim Dyn* 41(9-10): 2427-2438.

## SUPPLEMENTARY MATERIAL

**Figure S1.** Map of the Antarctic sectors (modified version from Goursaud et al. 2019).

**Figure S2.** Backward trajectories cluster analysis (10-days) by season: air-mass flow pattern for six sites in West Antarctica (S10, S20, S30, S50, S70, and S80) throughout the 2014 year.

**Figure S3.** Criteria for the classification of the air masses as their nature (continental or oceanic).

**Figure S4.** Contribution of the oceanic and continental air masses (in percentage) along the route of the BR-WAIS Traverse for the dry season.

**Figure S5.** Map of some basins from ABS and WS sectors showing the locations where the measures of the distance to the coast.

**Table S1.** Data of the 92 surface snow samples collected in the 2015 BR-WAIS Traverse (in the upstream areas of the MIS, IIS, PIG basins).

**Table SII.** Data of the total precipitation from the ERA5 reanalysis for eleven selected points (S01, S10, S20, S30, S40, S50, S57, S58, S70, S80, and S92).

**Table SIII.** Data of the possible number of clusters and percent change of TSV for all trajectories in both dry and wet months during 2014 that arrived at the ten selected points (S01, S10, S20, S30, S40, S50, S58, S70, S80, and S92).

**Table SIV.** Slopes (a), intercepts (b), uncertainties (u) and determination coefficients ( $R^2$ ) of the linear regression analyses between the stable isotopic compositions ( $\delta^{18}\text{O}$ ,  $\delta\text{D}$ , d) and geographical parameters (latitude (Lat.), long (Long.), altitude (Alt.) and distance to the coast (Dist.)) by transect – N-S Transect (1), N-S Transect (2), and E-W Transect (3).

**Table SV.** The isotopic results ( $\delta^{18}\text{O}$ ,  $\delta\text{D}$  and d) and geographical information (latitude, longitude, and altitude) of the 13 samples (1 m) from the 1990 International Trans-Antarctic Expedition (ITAE) used in this work.

**Table SVI.** Seasonal distribution of the 2014 snowfall for eleven sites of the BR- WAIS Traverse.

#### How to cite

MARCHER A, BERNARDO RT, SIMÕES JC & AUGER J. 2022. Water stable isotopes in snow along a traverse of the West Antarctic Ice Sheet: insights into moisture origins, air-masses distillation history, and climatic value. *An Acad Bras Cienc* 94: e20210353. DOI 10.1590/0001-3765202220210353.

*Manuscript received on March 10, 2021;  
accepted for publication on January 4, 2022*

**ANDRESSA MARCHER<sup>1</sup>**

<https://orcid.org/0000-0003-2680-1757>

**RONALDO T. BERNARDO<sup>1</sup>**

<https://orcid.org/0000-0002-1143-7916>

**JEFFERSON C. SIMÕES<sup>1,2</sup>**

<https://orcid.org/0000-0001-5555-3401>

**JEFFREY AUGER<sup>1,2</sup>**

<https://orcid.org/0000-0002-2304-2292>

<sup>1</sup>Universidade Federal do Rio Grande do Sul, Centro Polar e Climático, Instituto de Geociências, Av. Bento Gonçalves, 9500, 91501-970 Porto Alegre, RS, Brazil

<sup>2</sup>Climate Change Institute, University of Maine, Orono, ME 04469-5790, USA

Correspondence to: **Andressa Marcher**

E-mail: [andressa.marcher@gmail.com](mailto:andressa.marcher@gmail.com)

#### Author contributions

Andressa Marcher prepared the sample for analysis, performed stable isotopic analyzes on the WS-CRDS system (PICARRO® L2130-i, USA) at CPC/UFRGS Stable Isotope Lab under the supervision of Ronaldo T. Bernardo, organized and interpreted the isotopic data, modeled the backward trajectories in HYSPLIT model, extracted the snowfall data from Climate Reanalyzer.org data for eleven sites, did an interpretation the meteorological data integrated with isotopic results, and wrote the text of the article. Ronaldo T. Bernardo participated in the 2015 Brazilian WAIS traverse, collected the surface snow samples, supervised Andressa in the sample preparation process, supervised the isotopic analyses, participated in the interpretation of data, and reviewed this article. Jefferson C. Simões organized and coordinated the 2015 Brazilian WAIS traverse and revised this article. Jeffrey Auger constructed the temperature cross-sections of the troposphere using the solutions from ERA5 reanalysis and contributed to the interpretation of data.

